PHYSICAL REVIEW B VOLUME 54, NUMBER 24 15 DECEMBER 1996-II

Photoelectron spectroscopy of strongly correlated Yb compounds

J. J. Joyce, A. B. Andrews, A. J. Arko, R. J. Bartlett, and R. I. R. Blythe*
Los Alamos National Laboratory, Los Alamos, New Mexico 87545

C. G. Olson, P. J. Benning,† and P. C. Canfield
Ames Laboratory, U. S. Department of Energy, Ames, Iowa 50011

D. M. Poirier‡
Department of Chemical Engineering and Materials Science, University of Minnesota, Minneapolis, Minnesota 55455

(Received 29 November 1995; revised manuscript received 30 August 1996)

The electronic properties of the Yb compounds $\mathrm{YBCu_2Si_2}$, $\mathrm{YBAgCu_4}$, and $\mathrm{YbAl_3}$ along with purely divalent Yb metal, have been investigated by means of high-resolution ultraviolet and x-ray photoelectron spectroscopy. We present the intrinsic characteristic features of the $4f$ levels of Yb while accounting for lattice vibrations and the manifestation of corelike energy levels degenerate with the valence states and modified by the temperature-dependent Fermi function. For these strongly correlated Yb-based compounds, the hole occupancy values ($n_f \sim 0.6$) directly obtained from integration of the divalent and trivalent portions of the $4f$ photoemission features indicate that these compounds are strongly mixed valent. The small intensity modulation with temperature in the divalent Yb $4f$ levels (0–10 % over a $T = 20 - 300$ K range) is discussed within the conventional framework of the photoemission process and nominal allowances for lattice variations with temperature. Results from photoemission experiments on the divalent $4f$ levels of strongly correlated Yb compounds are remarkably similar to the $4f$ levels of purely divalent Yb metal. [S0163-1829(96)03748-4]

I. INTRODUCTION

The electronic properties of strongly correlated materials span the region between localized (corelike) and itinerant (bandlike) electronic states. A great many of the measured strongly correlated materials contain lanthanide elements and indeed, it is the $4f$ energy level of the lanthanides that dominates the electronic structure of these materials. Photoelectron spectroscopy (PES) has long played a central role in the measurement of the electronic properties of elemental lanthanides,[1] as well as strongly correlated compounds and alloys,[2,3] and often made a significant contribution to the acceptance or rejection of electronic-structure theories and model calculations.[4–6] In this paper we report the dominant effects of the photoemission process as they pertain to electronic properties of lanthanide materials (Yb, $\mathrm{LaCu_2Si_2}$, and $\mathrm{LuAl_3}$) as well as correlated electron materials ($\mathrm{YbAl_3}$, $\mathrm{YbCu_2Si_2}$, and $\mathrm{YbAgCu_4}$). In particular, we investigate the roles of phonon broadening and the Fermi function on the $4f$ energy levels of Yb and Yb compounds, where the $4f$ levels are in close proximity to the Fermi level (E_F).

The prominent role of PES in lanthanides and correlated electron materials studies arises from the interdependence between the PES measured energy distribution curves (EDC's) and the determination of the density of states (DOS) of the material.[7–9] For free-electron-like metals[8] and semiconductors[7] the EDC's have been successfully linked with the DOS of the material. Unfortunately, many of the simple assumptions or approximations one often invokes in order to relate the DOS of a material to the experimental EDC's are often inadequate for $4f$ levels and correlated electron materials in general. The first casualty of correlated electron systems is the one-electron approximation, which allows one to associate the EDC with the ground-state N-electron configuration of the solid. The one-electron approximation, along with assumptions regarding cross-sectional variations for different orbital angular momentum components and final-state matrix element effects, occasionally is invoked in a simplified treatment to reclaim the DOS from the experimental EDC. Of course a rigorous treatment of the photoemission process even for simple (free-electron-like) metals requires a many-body treatment and additional complications in relating EDC spectral features to the ground-state DOS (the orthogonality catastrophe[10] cautions against a simplistic comparison between the excited and ground states). Without the one-electron approximation matters quickly become untenable and thus several research groups have resorted to actual $(N-1)$-electron excited-state calculations for correlated electron systems and treat the electron correlations as the controlling factor in determining the electronic properties.[4–6] Other research groups have accounted for electron-electron interactions by modifications to more conventional calculations to arrive at the electronic structure.[11,12] The battles over which theory or model more correctly represents the electronic properties of lanthanides, actinides, and strongly correlated electron materials have been waged in other arenas.[13–20] This paper is concerned with the measurement of the $4f$ energy levels of Yb by means of photoelectron spectroscopy and the subsequent analysis of PES data in terms of well-understood photoemission principles.

We have studied the temperature evolution and line-shape characteristics of the Yb $4f$ levels in detail. In addition, we present surface studies of single-crystal Yb compounds that show multiple surface terminations or reconstructions in an effort to quantitatively separate the surface and bulk charac-

0163-1829/96/54(24)/17515(21)/$10.00

teristics of the divalent Yb 4f emission. Also, measurements for isoelectronic counterparts to the Yb compounds ($LaCu_2Si_2$ for $YbCu_2Si_2$ and $LuAl_3$ for $YbAl_3$) are included to determine the portion of the primary PES signal that arises from non-4f level electron emission. In addition to the high-resolution ultraviolet photoelectron spectroscopy (UPS) measurements made at photon energies between 60 and 120 eV, x-ray photoelectron spectroscopy (XPS) measurements at the Al K_α edge (1486.6 eV) for Yb compounds are also presented, which probe much deeper into the bulk of the crystal (probe depth up to 90 Å). XPS also provides an order of magnitude variation in photoelectron kinetic energy for consideration of time-dependent screening or relaxation mechanisms affecting the 4f PES spectrum. Furthermore, XPS provides verification of orbital angular characteristics and confirmation of divalent to trivalent 4f intensities (n_f) measured with UPS by providing different photoelectron cross sections for the valence and 4f states. The similarity between the 4f energy levels of purely divalent Yb metal and the divalent 4f levels of Yb-based strongly correlated (enhanced mass) compounds *as measured by PES*, show no indication of a spin fluctuation model [based on the single-impurity Anderson model[4–6] or (SIAM)] for interpretation of the electronic properties. At this time the PES results, in fact, are well described by conventional PES analysis methodologies.[13–15]

Moreover, it is now clear that the PES results of Ce-based correlated electron systems can also be explained in terms of conventional phonon broadening and temperature dependence of the Fermi function.[19,20] For Ce-based correlated systems, however, the 4f levels show periodicity with the lattice and appear to be very narrow bands within 50 meV of the Fermi level. In contrast to the 4f levels in Ce correlated electron systems, no periodicity with the lattice has yet been observed for Yb-based 4f energy levels. The similarities in the treatment of the 4f states between strongly correlated Ce and Yb-based materials, implied by particle (hole) [$4f^1$ ($4f^{13}$) in Ce (Yb)] symmetry,[6] are not observed in the PES measurements.[15] The principle similarity observed in PES between the 4f states of Ce and Yb-based correlated electron materials is a predictable temperature dependence of the 4f levels in the immediate vicinity of the Fermi level as phonon broadening and the Fermi function come into play with increasing temperature. The explanation of differences between the PES measured 4f energy levels and the electronic properties inferred from thermodynamic measurements on these materials awaits a suitable theory beyond the SIAM with its serious shortcomings.[13–16,19,20,31]

II. EXPERIMENT

Photoemission experiments were carried out at the Los Alamos U3C and AT&T Bell Laboratory U4B beam lines at the National Synchrotron Light Source, the Ames–Montana State ERG-Seya beam line at the Synchrotron Radiation Center and the University of Minnesota (Surface Science Instruments XPS capability with high-energy resolution and small spot size). The samples were primarily flux-grown single crystals ($YbCu_2Si_2$, $YbAl_3$, $LuAl_3$, and $LaCu_2Si_2$), with UHV *in situ* evaporated Yb films for the Yb metal and a slow-cooled stoichiometric melt in sealed Ta for $YbAgCu_4$ (coarse-grained polycrystalline). The samples were cleaved or evaporated in ultrahigh vacuum with a chamber base pressure of $(3–7)\times10^{-11}$ Torr. Temperature was controlled by placing the sample in direct contact with a cryostat cooled by either liquid helium, liquid nitrogen, or using a closed cycle He refrigerator. The UPS resolution was determined to be 60 meV at $h\nu=60$ eV and 45–95 meV at $h\nu=102$ and 120 eV for high-resolution studies (100 and 140 meV for moderate resolution studies). The XPS resolution was 450 meV at $h\nu=1486.6$ eV. The photoelectron spectra of the Yb 4f levels were enhanced by means of difference curves with isoelectronic lanthanides ($LuAl_3$ and $LaCu_2Si_2$) and by 4f photoelectron cross-section enhancement at selected energies (102 and 120 eV). The strongly correlated materials and associated characteristic temperatures (T_K or Kondo temperature within the SIAM) considered in this work were $YbCu_2Si_2$ ($T_K\approx40$ K), $YbAgCu_4$ ($T_K\approx100$ K), and $YbAl_3$ ($T_K\approx400$ K).

III. RESULTS AND DISCUSSION

In the figures that follow we show PES spectra of the 4f energy levels for several lanthanide materials. In order to compare spectra with different control parameters, in particular temperature, it is necessary to normalize the intensity between these spectra. Several methods of normalization are possible, each with its own merits and shortcomings. We have used shallow core-level spectra from the compounds taken with higher-order (second- and third-order) photon energies from the synchrotron and chosen optimal photon energies to place the normalizing spectral feature directly above (Si 2p in $YbCu_2Si_2$ and $LaCu_2Si_2$) or below (Al 2p in YbAl and $LuAl_3$) the valence band and 4f levels of the compounds.

For materials without ligand core levels accessible by higher-order photon energies, we use mesh current (photon flux) normalization or normalization on a prominent non-4f feature in the valence band. Combinations of these methods for single-crystal $YbCu_2Si_2$ show that, in this instance, the three methods—Si 2p (ligand core level), Cu 3d (non-4f valence feature), and mesh current normalization—yield similar intensities for the Yb 4f spectral features to within 5% or 10%. Mesh current normalization is, in principle, a temperature-independent means of comparing two different PES spectra. Comparisons between mesh current normalization and ligand core-level integrated area normalization show a spectral intensity loss of $\sim0-10\,\%$ of the integrated area when the temperature is increased from 20 to 300 K. This small intensity loss for the bulk EDC features might be attributable to a Debye-Waller-type effect on the photoelectron emission. In some cases the normalization on the ligand core level might show a smaller temperature dependence than mesh current normalization for the integrated spectra intensity variation in the Yb 4f level. This is possible if there is a reduction in the mean free path as the temperature increases. We are concerned primarily with the Yb 4f level integrated intensity and possible changes in this intensity above and beyond conventional, non-4f behavior. Therefore, the ligand core-level normalization method provides all the necessary information and does so in a more robust manner than flux normalization. The differences in the two normalization methods can be reconciled with high-quality data including both core levels and mesh current readings. For the majority of the paper we will use core-level normalization. The differences between core-level and photon flux normalization with the associated implications to mean-free-path arguments is discussed in Sec. III E of the paper as interpretation of the flux normalized areas is preliminary at this point.

A. Yb metal and simple $4f$ levels

We begin our discussion with an analysis of the corelike $4f$ states in Yb metal. Ytterbium metal is a purely divalent material with all of the $4f$ electrons residing in the $4f^{14}$ closed-shell initial-state configuration and with a final-state binding energy of approximately 1.2 eV below the Fermi level as measured by PES. Although the $4f$ levels are degenerate in energy with the valence electrons, the radial extent of the close-shell $4f$ wave function is small, the overlap with the valence states is likewise small, and the hybridization is limited (see Appendix A). Thus the Yb $4f$ levels are often treated as corelike[21] and the overlap with the valence electrons is minimal, allowing the interaction between these levels to be treated perturbatively. In Fig. 1 we show temperature-dependent PES results for thin-film Yb metal evaporated on a Ta substrate. The data were taken at two different temperatures, 25 and 250 K, with all other experimental parameters held fixed. This data set will illustrate several of the common characteristics of photoemission including temperature-dependent binding-energy shifts, phonon broadening with increasing temperature, and integrated area conservation with peak height reduction.

The middle and lower frames of Fig. 1 show the experimental data (shaded circles) along with the nonlinear least-squares fitting to the data.[22] For the line-shape analysis, the solid black line is the total fit, the dotted line is the bulk $4f$ component, and the dot-dashed line is the surface component of the fit. In addition to the bulk and surface component, we use a non-$4f$ component consisting of valence electron states coincident in energy with the $4f$ levels and an integral secondary background proportional to the primary electrons of higher kinetic energy (Shirley-type background).[23] We use a Doniach-Sunjic (DS) line shape for the natural linewidth (Γ_{DS}) as an asymmetric variation on the Lorentzian line shape to account for the low-energy electron-hole pairs at the Fermi level.[24] The DS line shape is then convoluted with a Gaussian to account for both instrumental broadening (ΔE_{ex}) as well as phonon broadening (ΔE_{ph}) with temperature.[25,26]

In Fig. 1, the experimental resolution was ~115 meV and the natural linewidth obtained from the nonlinear least-squares minimization is 100 meV for the bulk $4f_{7/2}$, 102 meV for the bulk $4f_{5/2}$, and 125 meV for the surface $4f$ components with a DS asymmetry parameter (α) of 0.067 for the bulk and 0.119 for the surface components.[27] The parameters were obtained by fitting the $T=25$ K data. It should be noted that the experimental resolution was believed to be 113 meV and the minimization routine arrived at a value of 117 meV, which leaves ~30 meV ''extra'' Gaussian width by quadrature and might be attributable to zero-point electronic phonon broadening in a Frank-Condon model.[26] Extracting small differences through a root-mean-square (rms) process is risky at best, so we simply state that the zero-point phonon broadening in this case is small to negligible (0–30 meV) for Yb metal. We also calculated the recoil phonon contribution[26] using the Debye temperature $\theta_D=118$ K for elemental Yb to arrive at a value of 11 meV for the recoil phonon contribution, again a negligible value given the natural linewidth for this material.

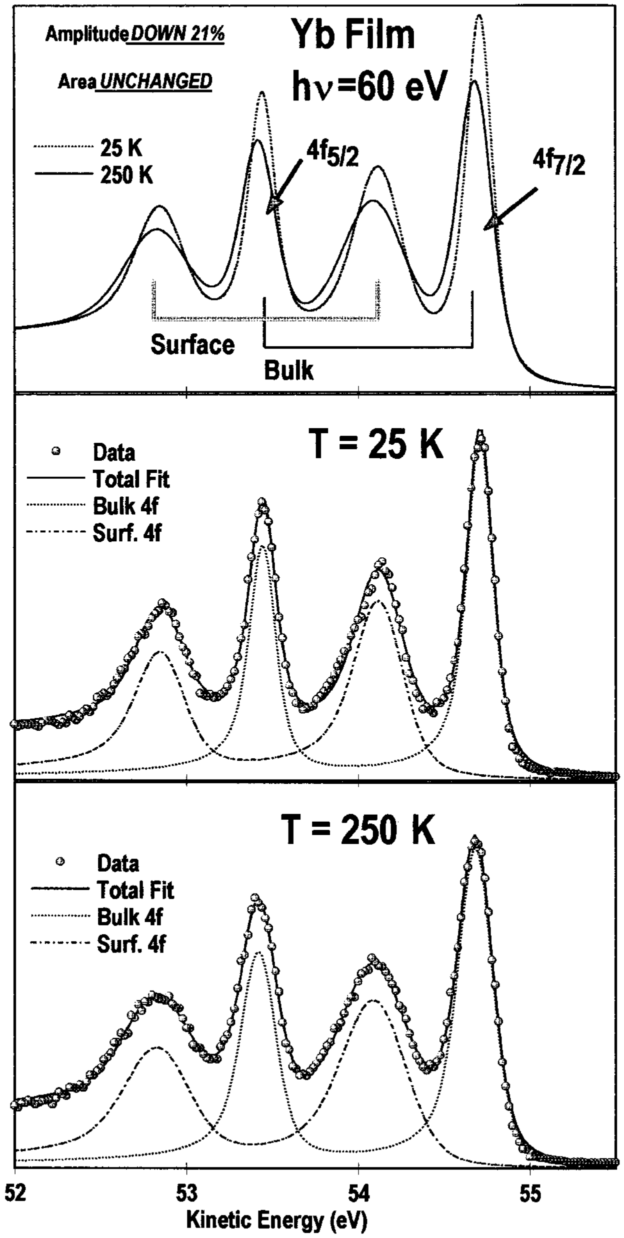

FIG. 1. Photoemission spectra in the UPS regime showing the temperature dependence of the Yb $4f$ levels in purely divalent Yb metal. The top frame shows the comparison of the fitted line shapes from the $T=25$ and 250 K data, while the middle and lower frames show the detailed line-shape analysis for the two temperatures. The shaded circles are the raw data, the thick solid line is the total fit to the data, and the bulk and surface components are represented by the dashed and dot-dashed lines, respectively. Note in the top frame how the peak intensity decreases by ~20% as the temperature is increased; however, the integrated area remains constant as the higher temperature data are broader due to phonon effects.

We next fit the $T=250$ K data in the lower frame of Fig. 1. It is clear that for both data sets the statistical fluctuations are small and the fits to the data are uniformly good. We therefore proceed to analyze the data by examining the fitted peaks for the two temperatures. The following two differences were observed in the 250-K fit with respect to the 25-K fit: first, the Gaussian broadening increased from 117 to 176 meV in the bulk components, resulting in a rms difference of ~ 130 meV attributable to phonon broadening; second, the energy of all four peaks shifted 25 meV to lower kinetic energy as the temperature increased. In the top frame of Fig. 1 we show the total fitted line shapes for both temperatures and note that both the shift in energy and the broadening of the spectral lines are plainly visible in the fitted data. Moreover, the integrated areas of the $4f$ levels were set equal for the two temperatures in Fig. 1 so that any amplitude reduction going from $T=25$ to 250 K must then be offset by an increased linewidth due to phonon broadening.

The binding energy shift in the Yb $4f$ data may be treated as arising from three contributions.[28] The first term arises from the change in the Fermi level with thermal expansion, the second term is due to a decrease in conduction electron density resulting in a reduction of the electrostatic potential in the atom, and the third term is a final-state contribution due to the temperature-dependent change in the relaxation energy. The phonon broadening of the measured PES line shape likewise arises from three terms.[25,26] The first term is the recoil broadening from the ejected photoelectron, which for large-Z ions and the low UPS kinetic energies becomes less significant (~ 11 meV for Yb metal); the second term is the zero-point phonon broadening due to differences in the nuclear coordinates of the ground-state atom and the photoexcited ion at $T=0$ K (0–30 meV from our analysis); and the third term is the temperature-dependent term due to electron-phonon coupling between the ground and excited states of an atom at a given temperature (~ 130 meV between 25 and 250 K) within the sudden approximation.[26] The third term, using the Debye model for solids, is proportional to θ_D for the material, the rms deviation of the atoms from the equilibrium position, and the square root of the temperature. It is the third term that dominates the EDC's for these large-Z compounds at low kinetic energies.

We next examine high-resolution $\Delta E_{\mathrm{ex}} \sim 50$ meV UPS and $\Delta E_{\mathrm{ex}} \sim 450$ meV XPS results for single-crystal YbAl_3 samples. The top frame of Fig. 2 shows the divalent Yb $4f$ emission for YbAl_3 taken at $h\nu=110$ and 50 meV resolution. The lower frame shows the bulk $4f_{7/2}$ and Fermi function region for this same fit in greater detail. The quality of the fit to the experimental data is once again seen to be uniformly good. The fitting methodology is as outlined above for Yb metal with the addition of the Fermi function entering into the fitting procedure as the Yb $4f$ levels are now very near the Fermi level. The addition of the Fermi function complicates the convolution process. In the absence of the Fermi function the experimental resolution and the phonon broadening terms are both well represented by Gaussians and one could add by quadrature these effects and then convolute a single Gaussian with the DS function to simulate the measured PES line shape. With the Fermi function and the noncommutativity of the convolution process, we must first convolute the natural linewidth (DS line shape) with a Gaussian for the phonon broadening, then multiply by the appropriate Fermi function, and finally convolute with another Gaussian representing the experimental resolution.

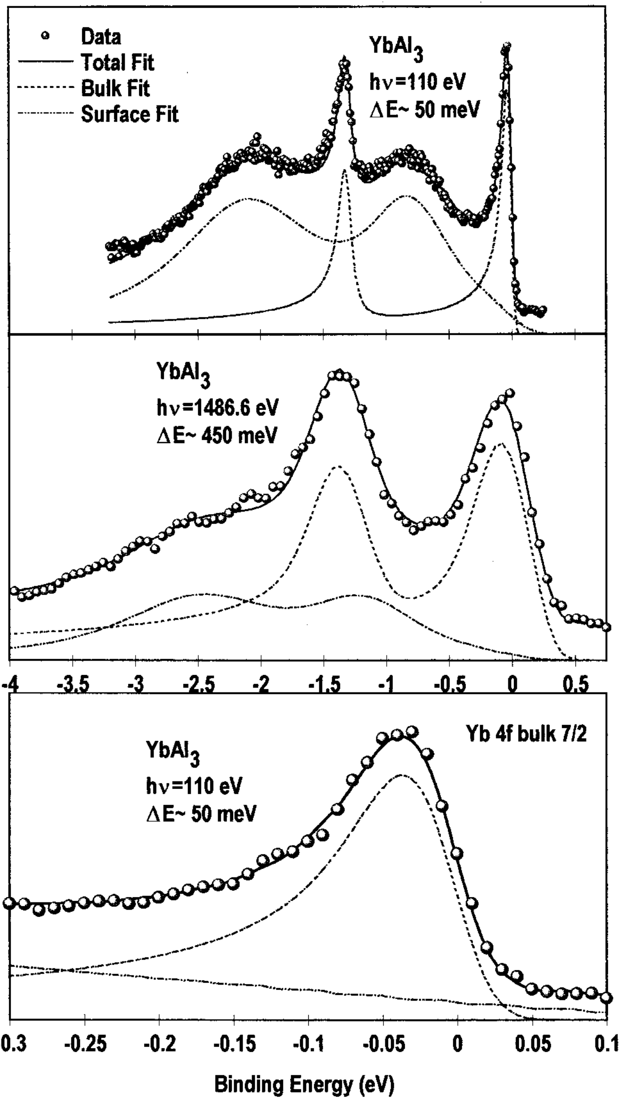

FIG. 2. Photoelectron spectra and line-shape analysis for YbAl_3. (a) YbAl_3 UPS data with 50 meV energy resolution at $T=20$ K. As in the Yb film case, the $4f_{7/2}$ and $4f_{5/2}$ components are well resolved as are the surface vs bulk components. (b) YbAl_3 XPS data with 450 meV energy resolution. The bulk $4f$ features are enhanced with the greater MFP of the XPS photoelectrons. (c) Details of the UPS fitting shown in (a) about the region of the Fermi level and the bulk $4f_{7/2}$ component.

The fitting in the top frame for the UPS data shows the peak of the bulk $4f_{7/2}$ level to be 21 meV below the Fermi level with a natural linewidth of 73 meV and asymmetry $\alpha=0.218$. The bulk $4f_{5/2}$ level has a natural linewidth $\Gamma_{\mathrm{DS}}=89$ meV and the surface core-level shifts (SCS's) are ~ 790 meV below their bulk counterparts. The larger natural linewidth for the $f_{5/2}$ level compared to the $f_{7/2}$ level is consistent with the addition of an extra decay channel for the $f_{5/2}$ level in traditional core-level spectra. This added decay channel is the Coster-Kronig process using the $f_{7/2}$ level, which is, of course, not available to an $f_{7/2}$ photohole. The additional channel reduces the photohole lifetime and consequently increases the linewidth. The applicability of this mechanism for $4f$ photohole decay in Yb compounds so near the Fermi level has not been quantitatively established. The binding energy of 21 meV below the Fermi level for $T \sim 20$ K is ~ 40 meV less than values we had quoted previously for $T \sim 80$ K.[15,29] While the binding-energy shifts between 20 and 80 K, it is not clear how much of the difference is attributable to temperature and how much is attributable to uncertainty in the fitting procedure, with the nonorthogonality of the DS, Gaussian, and Fermi function line shapes, the binding energy presents a serious challenge for exact determination. We use the current value of 21 meV throughout this paper since the data of Fig. 2 are the highest resolution data we have available for fitting $YbAl_3$ and the statistics are excellent.

The surface component now comprises a larger portion of the total $4f$ divalent signal than in the case of Yb metal, as the bulk $4f$ signal in $YbAl_3$ is split between divalent ($4f^{14}$) and trivalent ($4f^{13}$) configurations, whereas the Yb $4f$ atoms at the surface are all in the divalent configuration. In the middle frame of Fig. 2 we show XPS results for $YbAl_3$ and the associated line-shape analysis. We use the same fitting parameters as determined above for the UPS results, but now the ΔE_{ex} is 450 meV and the SCS is slightly larger for a different surface configuration as explained later in Fig. 6(c). Also, the surface component has diminished in intensity reflecting the larger mean free path (MFP) of the photoelectrons at ~ 1500 eV as opposed to the ~ 100-eV photoelectrons in the UPS regime. In fact, the surface contribution would have been even smaller if the sample were oriented normal to the electron analyzer but geometric considerations for sample surface preparation dictated a $\theta = 40°$ takeoff angle between sample surface and analyzer. The MFP geometric term goes as the cosine of θ. The takeoff angle used for $YbCu_2Si_2$ results in the second half of this paper was near normal and the surface contribution is proportionately smaller for those measurements.

The use of the same fitting parameters in the XPS and UPS regimes indicates that the UPS measurements are indeed coupling to the bulk states of the solid effectively and are measuring the bulk properties of the material in the UPS as well as the XPS modes. Also, the same linewidth and asymmetry parameters being valid in the UPS as well as the XPS regimes where the photoelectron kinetic energy varies by a factor of 15 and the time frame for photoelectron interaction with the photohole in the solid varies by nearly a factor of 4 gives an indication that the sudden approximation is most probably valid in both cases. This is a useful assumption for direct application of the Frank-Condon principle using vertical nuclear coordinate excitation in the temperature-dependent electronic phonon broadening of solids.

One note of caution is required with the introduction of the Fermi function. Whereas the Lorentzian (or DS) vs Gaussian character of a PES line shape could be determined rather accurately with data of sufficiently good statistics,[26,30] the introduction of the Fermi function further increases the nonorthogonality of the basis functions for the minimization process and can lead to nonuniqueness in the solution set. A strict adherence to reasonable limits in the parametric starting values and acceptance only of output parameters that realistically could represent the physics of the photoemission for the material measured should limit the solution sets to reasonable values.

B. Effects of temperature

In order to quantify the effects of the Fermi function and phonon broadening for the $4f$ levels degenerate with the Fermi level, we have constructed a simulation of temperature-dependent characteristics for $4f$ photoemission with parameters based on the values found in Fig. 2 for $YbAl_3$ and Fig. 1 for Yb metal. The simulation is as follows. We take the binding energy (21 meV), linewidth ($\Gamma_{DS7/2} = 73$ meV, $\Gamma_{DS5/2} = 89$ meV), asymmetry ($\alpha = 0.218$), and spin-orbit splitting (1.29 eV) from the $YbAl_3$ fitting at $T = 20$ K in Fig. 2, combine this with the Yb $4f$ temperature dependence (~ 130 meV from phonon broadening between 20 and 300 K) of Fig. 1, and finally include the appropriate Fermi function for a given temperature T. In the top frame of Fig. 3 we show the simulated effects on the $4f$ energy levels at 20, 80, and 300 K with an experimental resolution of 45 meV. In the middle frame we show the details of the top frame for the region around the $4f_{7/2}$ and the Fermi level.

Several points of interest should be noted. First, the integrated intensities of the three different temperatures were normalized on the $4f_{5/2}$ component by setting the areas equal in the region between -2 and -1 eV. The line-shape development with temperature of the $4f_{5/2}$ level is very similar to the temperature results reported in Fig. 1 for Yb metal, with the amplitude of the peak decreasing with temperature, but the peak simultaneously broadening out to maintain a constant area. Next, the same amplitude reduction and line-shape broadening occurs in the $4f_{7/2}$ peak near the Fermi level, but now the Fermi function begins to truncate more and more of the spectral intensity as the influence of the Fermi function extends further beyond the zero-energy reference with increasing temperature. Moreover, the effects of the Fermi function on truncating spectral intensity are further enhanced by the increased phonon broadening of the $4f_{7/2}$ line shape centered just below E_F, which tends to push even more spectral weight toward the Fermi level with increasing temperature. The end result as demonstrated in the middle frame is a sizable loss in peak amplitude, an apparent shift in the peak position away from the Fermi level with increasing temperature, and an actual loss in $4f_{7/2}$ spectral intensity with temperature. The lower frame in Fig. 3 demonstrates that this effect is still readily observable at the more common experimental resolution of 100 meV.

Conservation of charge discourages an actual loss in total intensity with temperature so one might expect compensating effects in the Yb compound data that will allow for conservation of charge with temperature by introducing mechanisms not included in the simulation. Several mechanisms are possible. First, some of the $4f$ electrons near the Fermi level could be converted to non-f conduction electrons with increasing temperature (spectroscopically observed as divalent $4f$ electrons being converted to trivalent $4f$ electrons) or the divalent $4f$ levels at the Fermi level can be shifted to

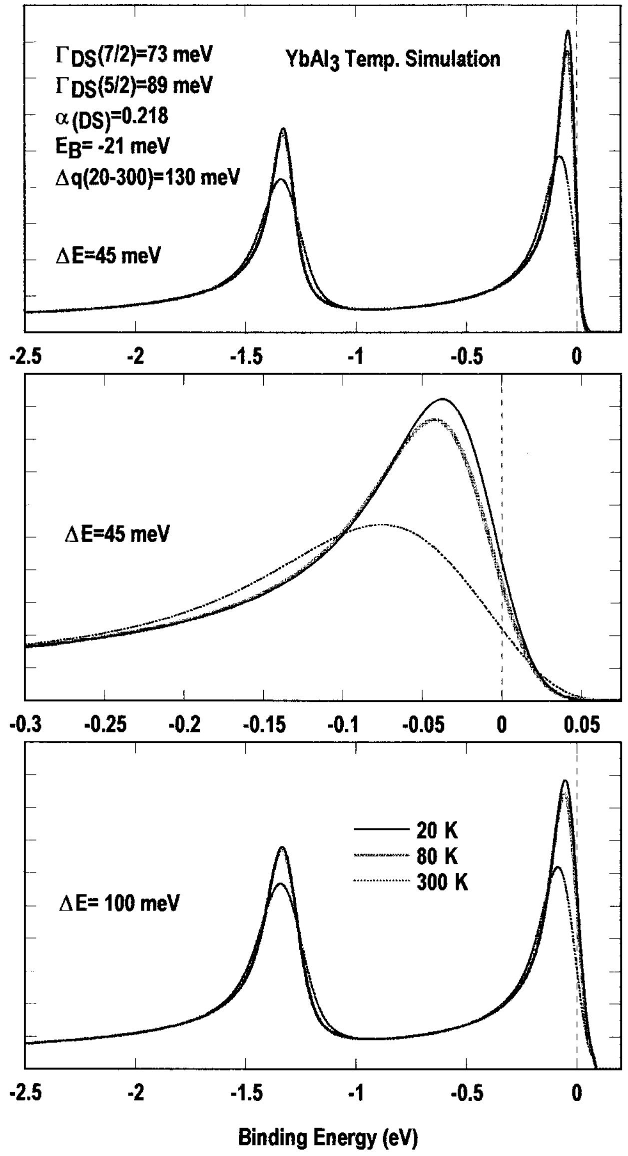

FIG. 3. Simulation of the effects of the Fermi function and phonon broadening with increased temperature. The natural linewidth, binding energy, and asymmetry are from the fitting of the high-resolution YbAl$_3$, data in Fig. 2. The top and bottom frames show two different experimental resolutions, 45 and 100 meV. A 130-meV Gaussian phonon broadening (20–300 K) and the appropriate Fermi function represent the temperature dependence in the simulation. The phonon broadening is the same as that for the Yb film in Fig. 1. The center frame is a detail for the $4f_{7/2}$ and Fermi level region of the $\Delta E_{\mathrm{ex}}=45$ meV simulation.

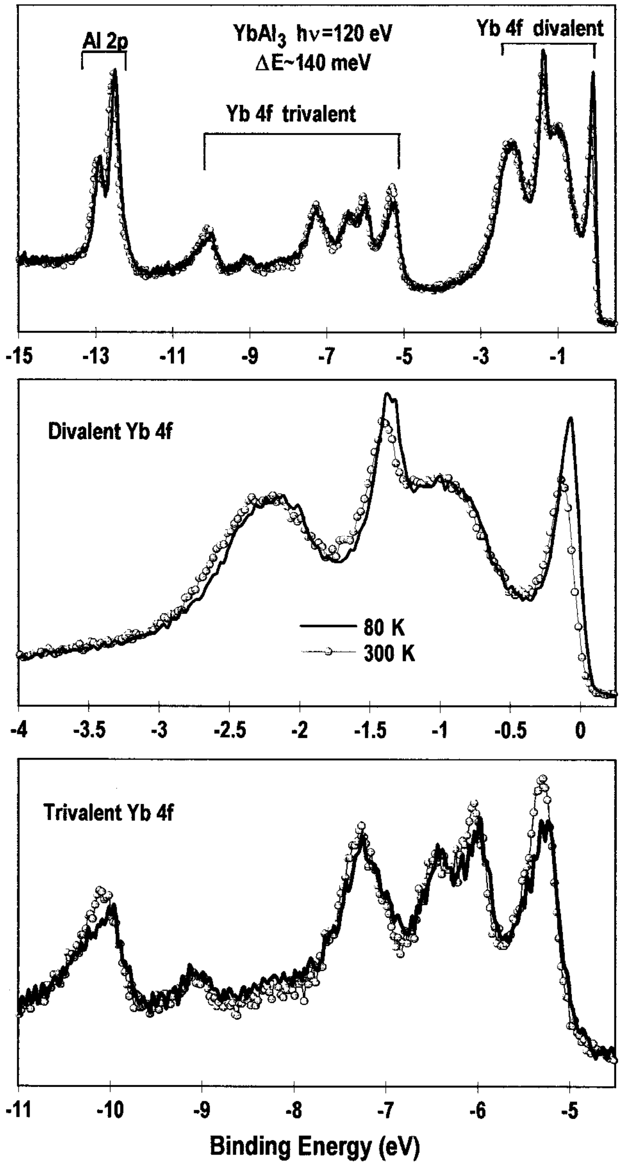

FIG. 4. UPS data for YbAl$_3$, taken at 80 and 300 K, showing the entire valence band and the Al $2p$ core level from high-order synchrotron photons in the top frame with details of the divalent and trivalent portions of the $4f$ emission in the center and lower frames, respectively. The spectra are normalized on the integrated area of the Al $2p$ core level with an experimental resolution of ~140 meV.

higher binding energy with increasing temperature, thereby reducing the effects of the Fermi function on the integrated spectral intensity.

In fact, these mechanisms are apparently realized in the PES data below. The energy shift in the PES data away from the Fermi level with increasing temperature is not unique to $4f$ photoemission and is in fact a general trend realized in most materials. While the energy shift with temperature may serve to reduce the amount of spectral weight lost in our $4f$ simulation, it would generally not be considered a driving force for the energy shift. The conversion of divalent to trivalent $4f$ electrons with increasing temperature could certainly compensate for spectral weight loss in the vicinity of the Fermi level.

C. YbAl$_3$

Temperature-dependent PES results for the entire valence band of YbAl$_3$, along with the Al $2p$ level used for normalization purposes, are presented in Fig. 4. The data were taken at temperatures of 80 and 300 K. In the top frame we show the entire valence band including the divalent and trivalent Yb $4f$ emissions with the Al $2p$ core level just below the trivalent Yb emission. The monochromator for this experiment was set for an energy of 60 eV, but with higher-order light we collected PES spectra in the kinetic-energy range from 100 to 117 eV. This energy interval yields second-order photons ($60\times 2=120$ eV) appropriate for the Yb valence band (starting at $h\nu-\phi$, where ϕ is the work function, and ending 12 eV below the Fermi level) as well as third-order photons ($60\times 3=180$ eV) for the Al $2p$ level [the binding energy (E_n) for the Al $2p$ is ~ 72 eV, so that $180-E_B(\text{Al } 2p)-\phi=103.5$ eV kinetic energy or 13 eV below the second-order Fermi level]. This seemingly complex method of using higher orders of diffracted light from the synchrotron provided a most convenient method for normalizing the $4f$ emission of the temperature-dependent Yb $4f$ levels in YbAl_3.

We have normalized the integrated area of the Al $2p$ core levels for the data at the two temperatures presented in Figs. 4 and 5. Several points can be made from the data in Fig. 4. First, there is a shift toward greater binding energy in the data as the temperature is increased from 80 to 300 K. This shift is observed in the Al $2p$ core level with a binding energy of 72 eV as well as the Yb $4f$ levels in the valence band. The shift is not unique to rare-earth compounds or heavy fermions; it is a general manifestation of the temperature-dependent processes described in Sec. III A. The middle frame of Fig. 4 shows the details of the Yb $4f$ divalent region (-4 eV to E_F), while the lower frame shows the $4f$ trivalent region (-12 to -4 eV). Second, from the lower two frames there is an apparent reduction in the divalent intensity as the temperature increases with a commensurate increase in the trivalent intensity over the same temperature interval. Finally, it should be noted that the temperature dependence of the divalent region in the middle frame shows a striking resemblance to the simulation in Fig. 3 of a $4f$ core level cut by a Fermi function and broadened with temperature by phonons.

In Fig. 5 we show the quantitative line-shape analysis for the data presented in Fig. 4. While the data of Fig. 4 for YbAl_3 are by no means our highest-resolution temperature-dependent data for this system, they have several merits including the following: (i) they encompass the entire divalent and trivalent $4f$ emission for Yb; (ii) they include the Al $2p$ levels from higher-order photons for normalization; and (iii) they contain sufficient data point density and counting statistics to provide a high confidence level in the quantitative analysis results. As such, this data set represents the most complete temperature-dependent YbAl_3 data available at this time. We have analyzed the divalent Yb $4f$ levels presented in the middle frame of Fig. 4 by the methods outlined for Yb metal (Fig. 1), as well as the high-resolution YbAl_3 (Fig. 2) in previous paragraphs. With $\Delta E_{\text{ex}}\sim 140$ meV for the data in Fig. 5, the fits to the data are indicated by the solid black lines with the data as shaded circles. It is observed that the fits are again uniformly good (small χ^2 value in the nonlinear least-squares minimization) and are consistent with the previous fits to the Yb $4f$ levels. In the top frame of Fig. 5 we show the bulk $4f_{7/2}$ and $4f_{5/2}$ components of the fits to the 80- and 300-K data. It is clear that the Yb $4f$ levels in YbAl_3 exhibit several of the features observed in the divalent Yb metal data. First, the $4f$ levels are shifted to lower energy by 48 meV as the temperature is increased from 80 to 300 K. Next, the $4f$ levels broaden (~ 100 meV) with increased temperature due to electron-phonon interactions just as in Yb metal. Finally, it should be noted that the $4f_{5/2}$ level amplitude is reduced by a smaller amount with increasing temperature compared to the $4f_{7/2}$ level, just as predicted by the simulation in Fig. 3, with the effects of the Fermi function and phonon broadening coming into play.

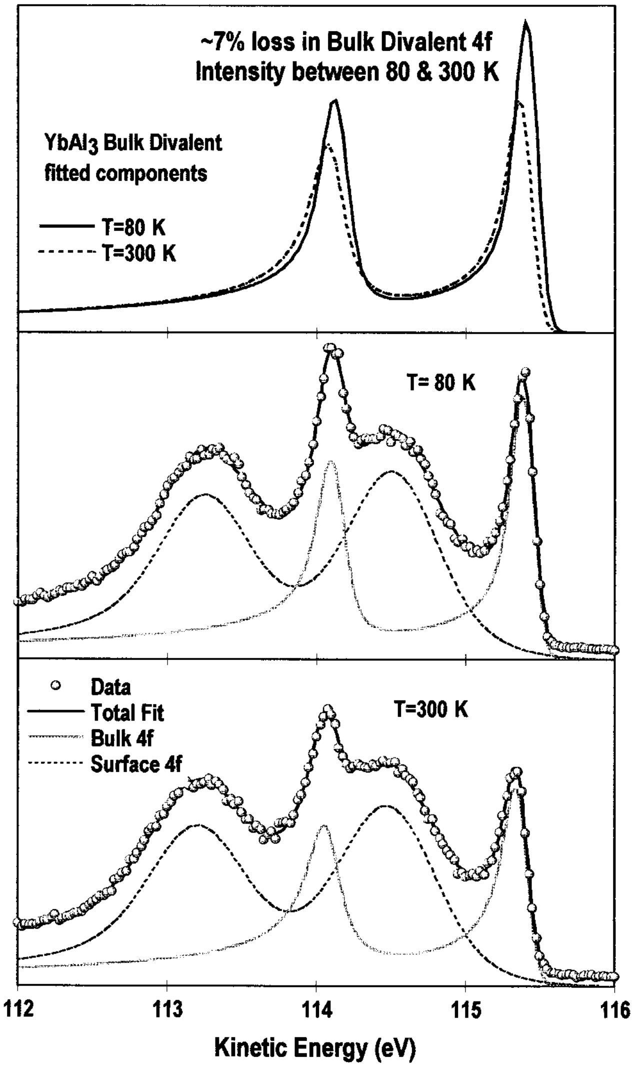

FIG. 5. Line-shape analysis for the divalent portion of the YbAl_3 spectra presented in Fig. 4 at $T=80$ and 300 K. In the lower two frames, the shaded circles are the raw data, the thick black line is the total fit, and the gray line and the dotted lines represent the bulk and surface components of the fit, respectively. In the top frame the bulk $4f$ components are compared at the two different temperatures, showing a 7% loss in integrated intensity from 80 to 300 K.

The total spectral weight loss for the bulk fitted divalent $4f$ levels in Fig. 5 is $\sim 7\%$ between 80 and 300 K. The loss in bulk divalent $4f_{7/2}$ spectral intensity could arise from materials considerations and/or spectroscopic considerations. The materials consideration would be the conversion of an f electron to a conduction electron (observed in the EDC as the conversion from divalent to trivalent intensity in the $4f$ level), whereas the spectroscopic phenomenon could arise from a reduction in the photoelectron mean free path with increasing temperature (phonon interactions, increased scattering), thereby allowing a shorter probe depth into the sample and reducing the PES signal attributable to the bulk $4f$ intensity. The latter effect would probably not be the entire explanation for a temperature-dependent intensity reduction, but might represent a significant portion of the effect. Moreover, when compared with the simulation in Fig. 3, the intensity reduction for 80–300 K in Fig. 5 for $YbAl_3$, (7%) is smaller than that in the simulation (12.5%). As indicated in the simulation discussion, an energy shift away from the Fermi level would be responsible for a compensating effect that lessens the intensity variation as a function of both phonon broadening and the Fermi function with increasing temperature.

In Fig. 6 we show details of the line-shape analysis for the Yb $4f$ levels of $YbAl_3$ in the top two frames as well as two different surface terminations for the same single-crystal cubic samples in the bottom frame. The data used in the top two frames are divalent $4f$ emission with $\Delta E_{ex} \sim 95$ meV from a $YbAl_3$ sample. We study the changes in parameters obtained when using two variations for the line shape representing symmetric and asymmetric fundamental line shapes for the oscillator strength of the $4f$ energy level. In the top frame of Fig. 6 we use a Lorentzian line shape to represent the fundamental functional dependence for the photoelectron spectrum. The Lorentzian line shape arises from the time-energy relation in representation theory for a discrete ground state using a time-dependent perturbation description of the photoemission process. The asymmetric line shape is based on the Lorentzian and is indeed recovered from the DS line shape as the asymmetry parameter α goes to zero. In addition to the fundamental oscillator description, the DS line shape accounts for the long-lived, electron-hole pairs very near E_F, which give rise to the skewed low-kinetic-energy side of the line shape characteristic of a metal with a large DOS at E_F. The bulk $4f_{7/2}$ and $4f_{5/2}$ levels are shown shaded in Fig. 6 with the asymmetry of the DS line shape apparent in the middle frame when compared with the symmetric Lorentzian line shape in the top frame. Both line shapes are convoluted with the same 80-K Fermi function and 95-meV Gaussian function.

Several points can be made from the fitting in the top two frames of Fig. 6. First, the fit to the experimental data is better for the asymmetric line shape than for the symmetric one as determined by the χ^2 values from the analysis. In particular, the symmetric line shape does not fit the data as well in the Fermi-level region on the leading edge of the bulk $4f_{7/2}$ peak, on the trailing edge of the same peak, and at the apex of the bulk $4f_{5/2}$ peak. Also, in order to achieve a reasonable fit with the symmetric peak, the width of the bulk peaks increases substantially from ~ 75 to ~ 140 meV for the bulk $4f_{7/2}$ component. It is also observed that the percentage of the total emission attributed to the bulk components is diminished when going from the DS to the Lorentzian line shape. The interplay between the natural linewidth Γ_{DS} and the asymmetry parameter α is apparent. Although the functional dependence between Γ_{DS} and α is not linear, it is direct. For any given data set, a reduction in one of the parameters requires an increase in the other value to compensate. While the quality of the fit to the data is not maintained by adjusting these parameters, the direct dependence (as in Fig. 6) is clear.

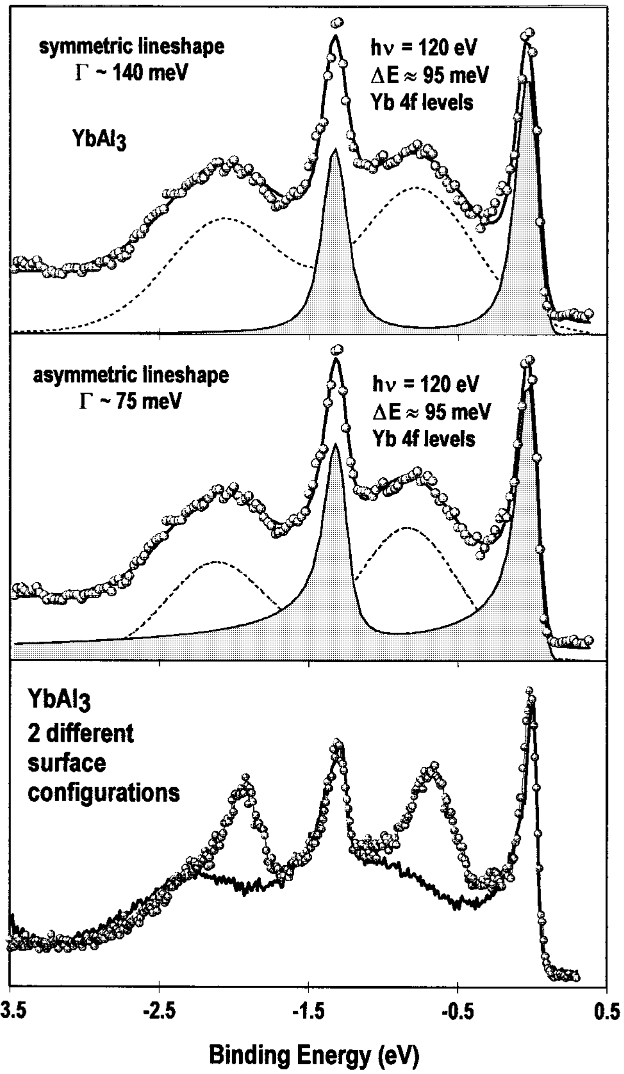

FIG. 6. Divalent portion of the $YbAl_3$ spectrum taken with 95 meV resolution is shown in the top two frames. The shaded circles are the raw data, the thick black line is the total fit with the shaded region, and the dotted lines represent the bulk and surface components of the fit. The top frame uses a symmetric Lorentzian line shape for the natural linewidth, which results in a poorer fit to the data than the asymmetric DS line shape used in the middle frame. In addition to a large χ^2 value in the minimization routine, the symmetric fit misses the data at the tail of the Fermi edge, high-binding-energy side of the bulk $4f_{7/2}$ peak and the peak of the bulk $4f_{5/2}$ component. The lower frame shows two different surface configurations for single-crystal $YbAl_3$ with substantially different surface component contributions to the overall divalent configuration.

The symmetry, or lack thereof, in the fundamental line shape also directly effects the magnitude of the secondary scattered background spectrum since the background function is calculated simultaneously with the primary peak features. In general, the background value increases as one goes to a more symmetric line shape since the ‘‘tail’’ of the fitted peak drops off faster as α tends toward zero. For a small region of any given valence band (say the Yb $4f$ divalent region), the use of a symmetric line shape would then reduce the overall intensity contribution for that spectral feature (bulk $4f_{7/2,5/2}$) in favor of background or contributions from other nearby spectral features. However, when the background function is applied over the entire valence-band region (divalent and trivalent together as in Fig. 7) and the same assumptions regarding line-shape asymmetry are made for the entire range of spectral features, the ratio of divalent to trivalent intensity comes out very nearly equal for the two different line shapes. The DS line shape appears to be the more suitable line shape for many Yb compound $4f$ levels ($\Gamma_{\mathrm{DS}}\sim 75$ meV, $\alpha\sim 0.2$) from the analysis presented in this paper (for Yb metal as reported in Fig. 1 we find $\Gamma_{\mathrm{DS}}\sim 100$ meV, $\alpha\sim 0.1$). Furthermore, the line shapes and linewidths obtained from the fitting in this paper are consistent with values obtained for the Lu $4f$ levels with a binding energy of ~ 6 eV (Refs. 16 and 31) in $\mathrm{LuAl_3}$ ($\Gamma_{\mathrm{DS}}\sim 83$ meV, $\alpha\sim 0.2$) as well as the Ta ($\Gamma_{\mathrm{DS}}\sim 40$ meV, $\alpha\sim 0.15$) (Ref. 32) and W ($\Gamma_{\mathrm{DS}}\sim 60$ meV) (Ref. 33) $4f_{7/2}$ levels with binding energies of ~ 22 and ~ 31 eV, leading to a fairly uniform picture of low-binding-energy $4f$ levels, which include the Yb $4f$ levels. Bearing in mind the interdependence of Γ_{DS} and α as noted in the description of the top two frames of Fig. 6, the uniformity in the common $4f$ level characteristics is reinforced.

The lower frame of Fig. 6 shows two different surface terminations for $\mathrm{YbAl_3}$. The two different terminations most likely represent a Yb-dominated surface termination (filled circles) and an Al-dominated surface termination (black line). Although the $4f$ surface components for the two different surfaces show distinct differences in both surface binding energy and surface $4f$ intensity, the bulk $4f$ levels in both cases are identical. That is, the binding energy and linewidth of the bulk $4f$ levels are unchanged by variations in surface termination; moreover, the bulk components are clearly separated energetically from the surface components regardless of surface termination. Along with the capability of fitting both UPS and XPS data with the same line-shape parameters, the above results indicate that the electronic structure rapidly converges to bulk values as one moves in from the surface and the states of the bulk couple efficiently to the surface in these single crystals allowing bulk characteristics to be readily observed with the limited mean free path obtainable in UPS photoemission.

In Fig. 7 we use the line-shape analysis discussed for Figs. 2 and 5 to separate the divalent $4f$ signal into surface and bulk components. In the top frame this is done for XPS, while the UPS valence band is separated in the middle frame. An iterative integral background is used over the entire valence band as previously described. By isolating the primary emissions in this manner, for both the trivalent and bulk divalent $4f$ signals, we are able to calculate the hole occupancy n_f for the $4f$ levels in $\mathrm{YbAl_3}$. The hole occupancy is defined as $n_f=I(f^{13})/[I(f^{13})+\frac{13}{14}I(f^{14}_{\mathrm{bulk}})]$, where $I(f^{13})$ is the integrated intensity of the primary trivalent $4f$ component and $I(f^{14}_{\mathrm{bulk}})$ is the integrated primary bulk divalent $4f$ component from the line-shape analysis [use of the symbol n_f for hole occupancy arises from the electron-hole symmetry between Ce and Yb heavy electron compounds; the original interest in Ce systems has dictated the nomenclature]. The value of n_f obtained for $\mathrm{YbAl_3}$ from the UPS and XPS data is ~ 0.63 with a range for UPS measurements of 0.6–0.65 obtained for many different cleaves on this material.[34]

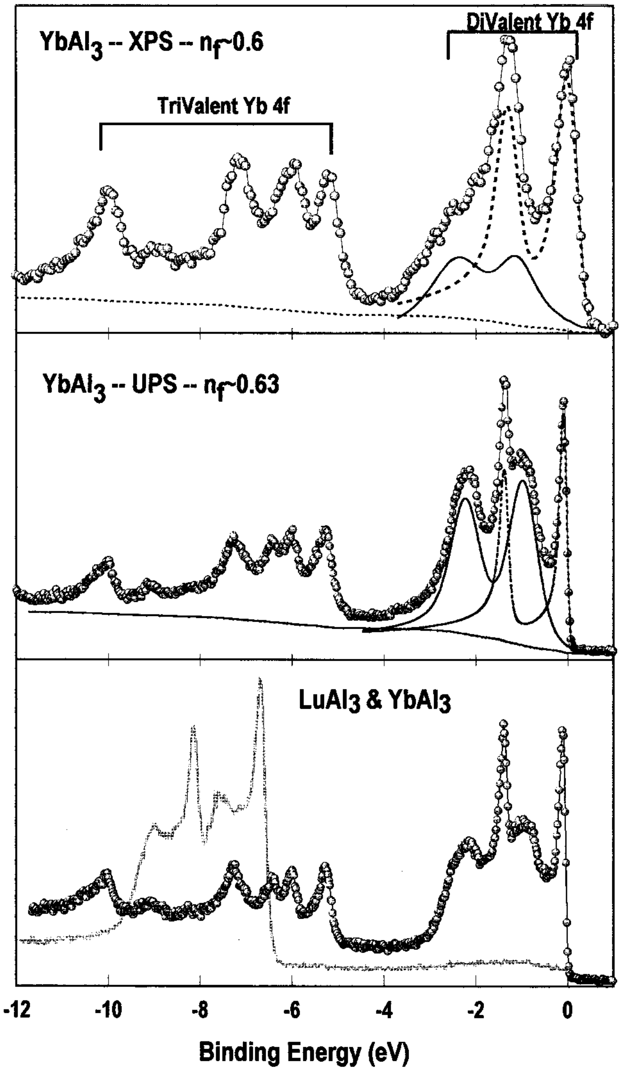

FIG. 7. (a) Full valence-band XPS data for $\mathrm{YbAl_3}$ showing the divalent and trivalent portions of the Yb $4f$ spectrum. The divalent $4f$ emission is separated into surface and bulk contributions as shown if Fig. 2 and then the bulk divalent and trivalent intensities are used to arrive at an $n_f\sim 0.6$ for $\mathrm{YbAl_3}$. (b) UPS data for $\mathrm{YbAl_3}$ with the same analysis method as above and again arriving at an $n_f\sim 0.63$ for $\mathrm{YbAl_3}$. (c) Normalized $\mathrm{YbAl_3}$ and $\mathrm{LuAl_3}$ UPS data. In addition to including a background component proportional to the primary emission of higher energy in our line-shape analysis, we account for the non-$4f$ component of the spectra by subtraction of a scaled Lu valence component that is seen to be both small and featureless in the Yb divalent region compared to the $4f$ signal at a photon energy of 120 eV.

The widest range for the n_f value for $\mathrm{YbAl_3}$ is obtained by allowing the asymmetry parameter in the divalent $4f$ line-shape analysis to vary between pure Lorentzian ($\alpha=0$) to $\alpha=0.25$, giving rise to n_f values ranging from 0.69 to 0.58, respectively. Previous indications (in Fig. 6) are that the use of a Lorentzian line shape for the natural linewidth in the divalent $4f$ signal leads to larger χ^2 values in the nonlinear least-squares analysis of the divalent data; thus the value of 0.69 sets an extreme upper limit for the hole occupancy in $\mathrm{YbAl_3}$ with 0.63 being the canonical value.[15,35,36] These n_f

values for $YbAl_3$ place this compound solidly in the mixed valent regime for theoretical treatment of the 4f energy levels.

In the lower frame of Fig. 7 we show the full valence band of $YbAl_3$ along with the Lu counterpart ($LuAl_3$) to this strongly correlated material. It is evident from these two spectra that the divalent Yb 4f levels very near E_F and the Lu 4f levels at ~6 eV below E_F share many common characteristics in the measured electronic structure. The quantitative similarities in the natural linewidth and asymmetry of the line shape already have been documented.[16] In addition to the obvious visual similarities, it is important to note that the non-f contribution to the measured electronic structure at a photon energy of 120 eV is both featureless and negligible on the scale of the 4f emission. This point is essential when undertaking the quantitative line-shape analysis of the divalent portion of the Yb 4f levels, as presented in Figs. 2, 5, and 6. For other materials, the non-f emission may not represent a negligible contribution.

D. $YbCu_2Si_2$

In the top frame of Fig. 8 we show UPS and XPS data for $YbCu_2Si_2$. This Yb compound has thermodynamic characteristics (low-temperature resistivity, heat capacity, and magnetic susceptibility) substantially different from that of $YbAl_3$, with a characteristic temperature of ~40 K compared with 400 K for $YbAl_3$. The characteristic temperature plays a central role in categorizing the role of the correlation between the f electrons in these heavy-fermion materials. We therefore proceed to quantitatively analyze the 4f excited-state emission of different Yb compounds to determine if systematics in the characteristic temperatures track with the 4f photoemission. The XPS data (shaded circles in the top frame of Fig. 8) show a much greater bulk to surface ratio in the divalent Yb 4f signal as the mean free path is increased by a factor of 3–4 over that of the UPS results (here the XPS data were taken at near normal emission between the sample and the electron analyzer so that the mean free path is maximum and even greater than the XPS $YbAl_3$ reported above). When differences in the Cu3d cross section and in the UPS vs XPS resolution are accounted for, the XPS and UPS data are fully self-consistent. Once again, these results confirm the coupling to true bulk states in UPS measurements and also the spatially localized nature of the Yb 4f surface components.

The treatment of the divalent Yb 4f emission in $YbCu_2Si_2$ at $h\nu = 102$ requires additional characterization in order to quantitatively separate out the non-4f component from the photoemission signal. In the middle frame of Fig. 8 we show full valence-band data for $YbCu_2Si_2$ and $LaCu_2Si_2$. The La compound is isoelectronic with the Yb compound, except for the Yb 4f levels, and has the same crystal structure. By taking spectra of both compounds with identical experimental setups including photon energy and then normalizing on the most prominent valence-band structure (Cu 3d levels), we are able to separate the Yb 4f emission from the non-f emission. Due to slight differences in atomic shell volumes and lattice parameters for the two materials we expanded the energy scale of the La compound by ~6% around the Cu 3d levels in order to have the sp bands of Si and Cu s bands extend to the $YbCu_2Si_2$ Fermi level (if we align the Fermi levels for the two materials then the Cu 3d emission is ~250 meV lower in binding energy for La than Yb and difference curves show nonphysical negative-valued amplitudes). In this manner were are able to account for the non-4f emission. However, the secondary emission is also different from the two spectra as the secondaries at en-

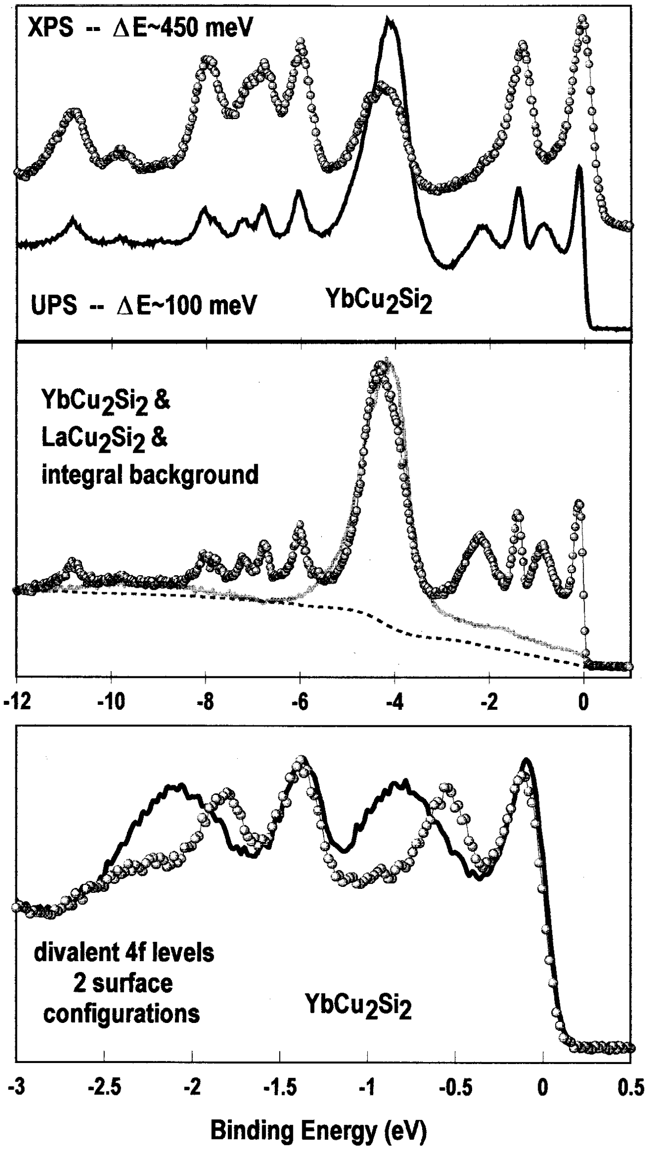

FIG. 8. (a) Valence-band data for $YbCu_2Si_2$ in the UPS regime ($h\nu = 102$ eV) with $\Delta E_{ex} \sim 100$ meV and the XPS regime ($h\nu = 1486.6$ eV) with $\Delta E_{ex} \sim 450$ meV. The different photon energies gives rise to differences in the Yb 4f and Cu 3d cross sections as well as differences in the photoelectron MFP as indicated by the smaller surface contribution in the XPS data for the divalent 4f surface signal. (b) UPS data for $YbCu_2Si_2$ and $LaCu_2Si_2$ at $h\nu = 102$ eV showing the non-4f contribution to the valence-band spectrum at this photon energy as well as the secondary background component for the data. (c) Two different single-crystal divalent $YbCu_2Si_2$ surface configurations showing variations in the crystal surface termination and the high-resolution UPS capability to distinguish surface configurations and bulk signal components.

ergy E_0 are proportional to the primary emission at $E>E_0$, which, in the case of the Yb compound (filled circles, middle frame Fig. 8), includes the Yb $4f$ signal, whereas the La compound does not.

We proceed as follows. A secondary background function is computed for each material and subtracted from the total signal. We then normalize the spectra on the Cu $3d$ emission and add the $YbCu_2Si_2$ secondary emission (dashed line) to the La primary emission spectrum to arrive at the total non-$4f$ emission (gray line). This composite La-background spectrum is again, as in the case for the $(R)Al_3$ (where R denotes rare-earth elements La, Yb, and Lu), both featureless and small compared to the divalent $4f$ emission near the Fermi level, although it is a larger percentage of the total emission than in the $(R)Al_3$ samples. In the lower frame of Fig. 8 we show two different $YbCu_2Si_2$ surface terminations that give rise to differences in the binding energy of the surface component with respect to the bulk $4f$ component, just as in $YbAl_3$. $YbCu_2Si_2$ is a layered material with stronger in-plane bonds than the interplanar bonds. As such, we attribute the two different surface configurations to Cu-dominated and Si-dominated surface layers with the Yb $4f$ electronic structure converging to its bulk configuration beyond the Yb layer nearest the surface. We have also observed what appeared to be a Yb surface-terminated plane on one cleave of $YbCu_2Si_2$. However, this surface was obtained only once out of dozens of $YbCu_2Si_2$ cleaves and appeared to be of a highly strained nature. As in the case for $YbAl_3$ (lower frame Fig. 6), the bulk components show the same binding energy, linewidth, and asymmetry parameter regardless of the surface termination.

We proceed with the same detailed line-shape analysis for the Yb $4f$ of $YbCu_2Si_2$ which was detailed for $YbAl_3$ in Figs. 2, 5, and 6. Again we are able to fit both the UPS and XPS data with two doublets (a bulk $4f_{7/2}$ and $4f_{5/2}$ pair and the surface counterparts), the only differences arising from the greater bulk sensitivity of the XPS data (the surface contribution was $\sim 11\%$ of the divalent emission vs $\sim 43\%$ for UPS), and the better energy resolution of the UPS vs XPS data (~ 100 meV vs ~ 450 meV). The results of this line-shape analysis are presented in Fig. 9 with XPS data in the upper frame and UPS data in the lower frame. Once again the fit to the data is good throughout the entire divalent region, as indicated by the χ^2 values and visual inspection of the fitted line shape (solid black line) to the experimental data (filled circles). The bulk component of the fit is indicated by the dashed line and the surface component by the dot-dashed line.

The $4f$ hole occupancy for $YbCu_2Si_2$ is calculated to be 0.63 ± 0.04 and the results of the analysis and calculation leading to this value are shown in the top frame of Fig. 10. The line-shape analysis for the XPS divalent Yb $4f$ levels of $YbCu_2Si_2$ from Fig. 9 are used along with the methodology of non-$4f$ emission determination from Fig. 8. We use the XPS data rather than the UPS data since the Cu $3d$ signal is much lower proportionally to the Yb $4f$ than in the UPS data and, the bulk sensitivity (and thus the confidence level in reducing errors from the surface contribution) of the divalent signal outweights the advantage of superior energy resolution in the UPS data. The removal of the Cu $3d$ signal from the UPS data could have a significant effect on the integrated area of the trivalent Yb $4f$ integrated area since the Cu $3d$ states are so much more intense than the trivalent $4f$ states at $h\nu = 102$ eV. By working at XPS energies this pitfall is eliminated and the hole occupancy is determined with a minimal amount of uncertainty. The XPS data in the top frame of Fig. 10 represent the current state of the art for correlated electron heavy fermion XPS data by combining single crystal samples with $\Delta E_{ex} \sim 450$ meV (resolving power greater than 3300 at $h\nu = 1486.6$ eV) and excellent counting statistics. As such, the n_f derived from Fig. 10 brings new information to discussions regarding the modeling of heavy-fermion compounds. Once again, the n_f of 0.63 for $YbCu_2Si_2$ places this system strongly in the mixed valent regime for modeling and theoretical considerations.

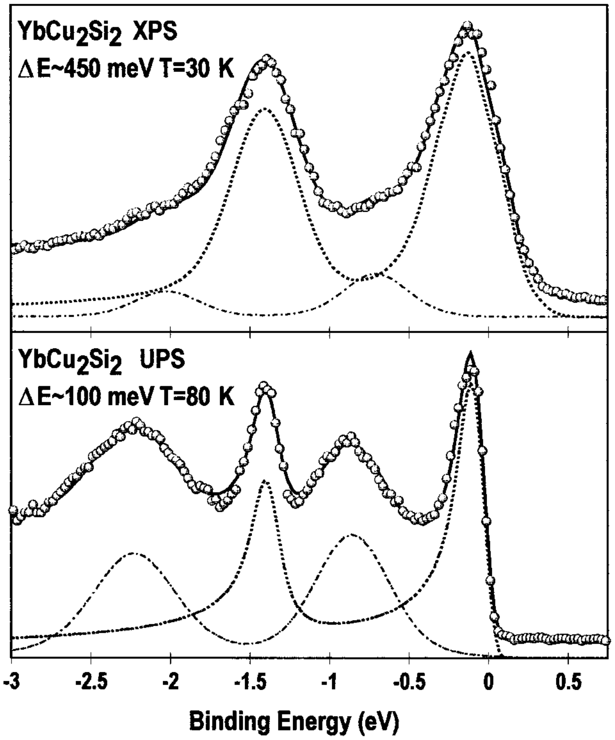

FIG. 9. Line-shape analysis for the Yb $4f$ divalent $YbCu_2Si_2$ data presented in Fig. 8. (a) XPS data and fitting showing the surface and bulk $4f_{7/2}$ and $4f_{5/2}$ components with an energy resolution of 450 meV. The bulk $4f$ components dominate the emission due to the long MFP at $h\nu = 1486.6$ eV. (b) UPS data and fitting with $\Delta E_{ex} \sim 100$ meV showing the total fit as well as the surface and bulk $4f$ contributions.

Not only is the n_f value for $YbCu_2Si_2$ very similar to that of $YbAl_3$, but the divalent $4f$ line-shape analysis also yields quite similar values. These findings would seem to be inconsistent with models for strongly correlated materials, which show scaling behavior (intensity, linewidth, and n_f) directly proportional to the characteristic temperature of a particular heavy fermion. In the lower frame of Fig. 10 we present temperature-dependent UPS data on $YbCu_2Si_2$. The data are normalized on the integrated area of the Si $2p$ core level just above the Fermi level arising from second-order photon excitations. We have removed the 50-meV binding-energy shift with temperature in order to better observe the normalization of the Si $2p$ level and the temperature dependence of the

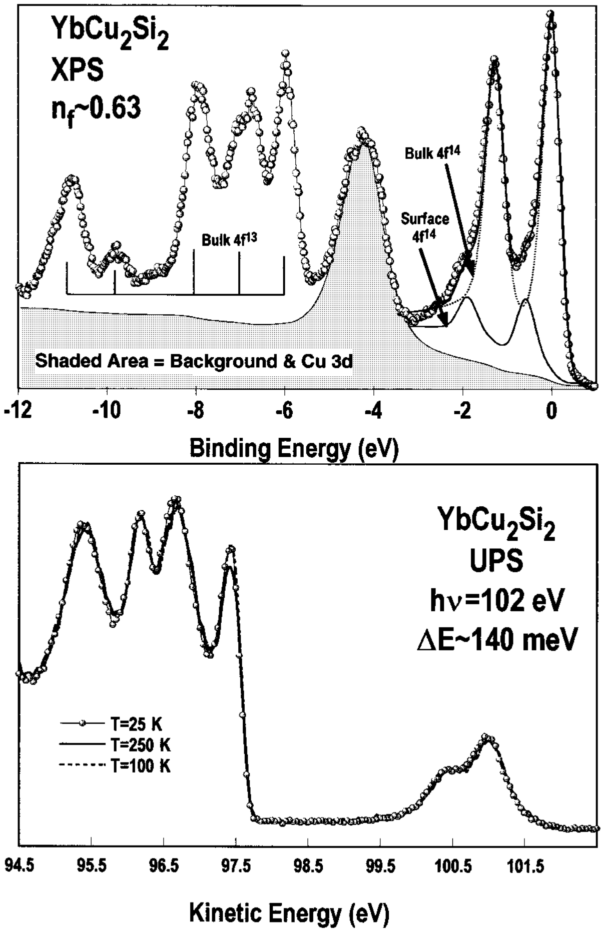

FIG. 10. (a) $YbCu_2Si_2$ XPS data showing the divalent and trivalent Yb $4f$ contributions as well as the Cu $3d$ and secondary background (shaded). The divalent $4f$ contribution is separated into bulk and surface contributions according to Fig. 9 and the bulk divalent to trivalent integrated intensity gives rise to an $n_f \sim 0.63$. (b) UPS temperature dependence of the divalent $YbCu_2Si_2$ $4f$ data between 25 and 250 K at $h\nu = 102$ eV. The Si $2p$ core level is shown in second order just above the Fermi level and the $2p$ integrated area was used for normalization of the $4f$ data.

$4f$ levels. It is obvious that the data show very little variation with temperature. In fact, the entire surface component doublet along with the bulk $4f_{5/2}$ level shows negligible temperature dependence. Only the bulk $4f_{7/2}$ level near the Fermi level shows any significant decrease with temperature and this is still small and most likely due to the role of the Fermi function at higher temperature as specified in the discussion related to Fig. 3 (phonon broadening of a sharp DOS in near proximity to the Fermi level). There are indeed variations in the temperature dependence of $YbCu_2Si_2$ data from cleave to cleave. Averaging over many cleaves, we have seen 0–10 % intensity loss over the 20–300 K temperature range for the bulk divalent Yb $4f$ signal. Since this is the same intensity variation observed for $YbAl_3$, where we presented a 7% decrease (Figs. 4 and 5), we now show data for $YbCu_2Si_2$ on the low side of the variational scale.

E. Yb compounds, single crystals, and the Fermi function

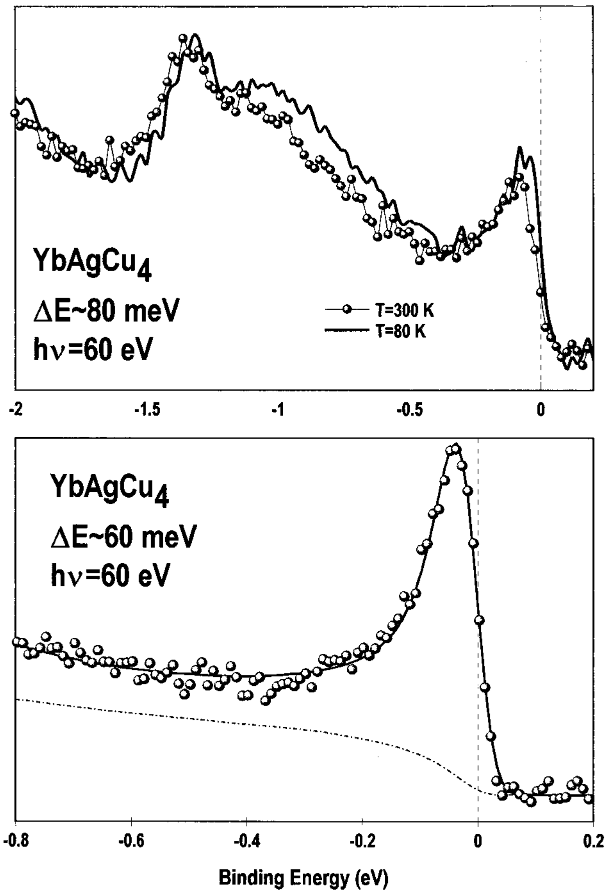

FIG. 11. (a) Temperature-dependent UPS data for $YbAgCu_4$ with $\Delta E_{ex} \sim 80$ meV for $T = 80-300$ K and showing the bulk $4f_{7/2}$ and $4f_{5/2}$ components along with the surface $4f_{7/2}$ component. There is a slight amplitude reduction in the bulk $4f_{7/2}$ component probably due to the Fermi function and a shift in the surface component with temperature. (b) $YbAgCu_4$ with $\Delta E_{ex} \sim 60$ meV for $T = 20$ K. The shaded circles are the data and the solid line is the fit to the data. The intrinsic linewidth for the bulk $4f_{7/2}$ component is 75 meV, which is in good agreement for the values obtained for Yb metal, $YbAl_3$ and $YbCu_2Si_2$.

The third strongly correlated Yb compound to be considered here is $YbAgCu_4$. Temperature-dependent data and line-shape analysis for this material are presented in Fig. 11. The top frame of Fig. 11 shows the temperature dependence (80–300 K) of the $4f$ levels within 2 eV of E_F. We have previously reported no temperature dependence below 80 K for this material.[29] The bulk $4f_{5/2}$ level is at -1.4 eV with the surface $4f_{7/2}$ level at -1 eV and the bulk $4f_{7/2}$ level inside of 100 meV of the Fermi level. The temperature dependence of the $4f$ levels for $YbAgCu_4$ follows the now common theme: (i) a slight (25–50 meV) energy shift away from the Fermi level with increasing temperature, (ii) little to no temperature dependence in the bulk $4f_{5/2}$ level, and (iii) a small temperature dependence in the bulk $4f_{7/2}$ level of a magnitude accounted for by the Fermi function and phonon broadening as modeled in the discussion for Fig. 3. In the lower frame of Fig. 11 we present high-resolution ($\Delta E_{ex} \sim 60$ meV) $T \sim 20$ K PES data (shaded circles) for the $YbAgCu_4$ bulk $4f_{7/2}$ level along with the nonlinear least-squares fit (solid black line) to the data. The line-shape analysis for this data shows $\Gamma_{DS7/2} = 73$ meV, $\alpha = 0.163$, and $E_B = 21$ meV. We reported these results for $YbAgCu_4$ in

Ref. 37 and subsequently, the line-shape analysis results have been confirmed by Weibel *et al.* with even better energy resolution $\Delta E_{\mathrm{ex}} \sim 20$ meV.[18] Clearly the line-shape analysis from these two works is not limited by the experimental energy resolution and the natural linewidth of the $4f$ spectral features is, in fact, about 75 meV, in remarkable agreement with the 75 meV natural width for YbAl_3 reported from our $\Delta E_{\mathrm{ex}} = 50$ meV data presented in Fig. 2.

High-resolution UPS ($h\nu = 102$ eV) results for YbAl_3 are presented in Fig. 12 with $\Delta E_{\mathrm{ex}} \sim 45$ meV in the top frame and $\Delta E_{\mathrm{ex}} \sim 75$ meV in the lower two frames. The filled circles are our single-crystal YbAl_3 data from this work and the solid black lines are polycrystal data digitized from Ref. 17. First and most importantly, the 45-meV data in the top frame of Fig. 12 show the bulk $4f_{7/2}$ level and clearly indicate that *the natural linewidth* ($\Gamma_{\mathrm{DS}7/2}$) *of the spectral feature is broader than the experimental resolution and both data sets are measuring the same fundamental line shape.* The difference between the data sets is mainly in the secondary electron contribution and the tail of the surface $4f_{7/2}$ level coming in on the high-binding-energy side from $E_B \sim 0.8$ eV. The single-crystal data show a larger peak to valley ratio than the polycrystal data, probably because the cleaved single-crystal sample has a flat and minimal surface area along with a low scattering cross section due to the periodicity of the lattice as well as strong coupling between the surface and bulk wave functions due to the single-crystal nature of the sample.

In the middle and lower frames of Fig. 12 we show the full divalent portion of the Yb $4f$ levels for YbAl_3. Both frames show the same two sets of data; the difference between the two frames is in the normalization of the data sets. In the middle frame the data are normalized on the amplitude of the bulk $4f_{7/2}$ level at the Fermi level, while in the lower frame the data are normalized on the amplitude of the surface components as well as the secondary emission. From the perspective of the middle frame, one would conclude that the polycrystalline sample had a larger surface component and more secondary scattering making up the total PES emission than the single-crystal data. From the perspective of the lower frame, one would conclude that the polycrystalline sample does not have as deep an escape depth or as efficient a coupling of the bulk states to the surface as the single-crystal data. In either event, it is clear that the peak to valley ratio of the PES signal is larger for the single-crystal data than for the polycrystal data. Also, the percentage of the total PES signal due to primary electron bulk $4f$ emission is larger for the single-crystal data than for the polycrystal data. Both of these facts reduce the magnitude of the uncertainty in the single-crystal data line-shape analysis and increase the confidence level in the nonlinear least-squares results over those of the polycrystal data. This is a general trend in PES data and underscores the advantages of working with single-crystal samples when they are available.

It should also be noted that analysis of the entire divalent $4f$ spectrum is far preferable to analysis of a limited portion of the spectrum, say, the bulk $4f_{7/2}$ level near E_F. Specifically, analysis of the full divalent spectrum restricts the magnitude of the secondary background function to physically realistic values not greater than the PES signal at greater binding energy than the divalent $4f$ levels.[15] Also, the fit to

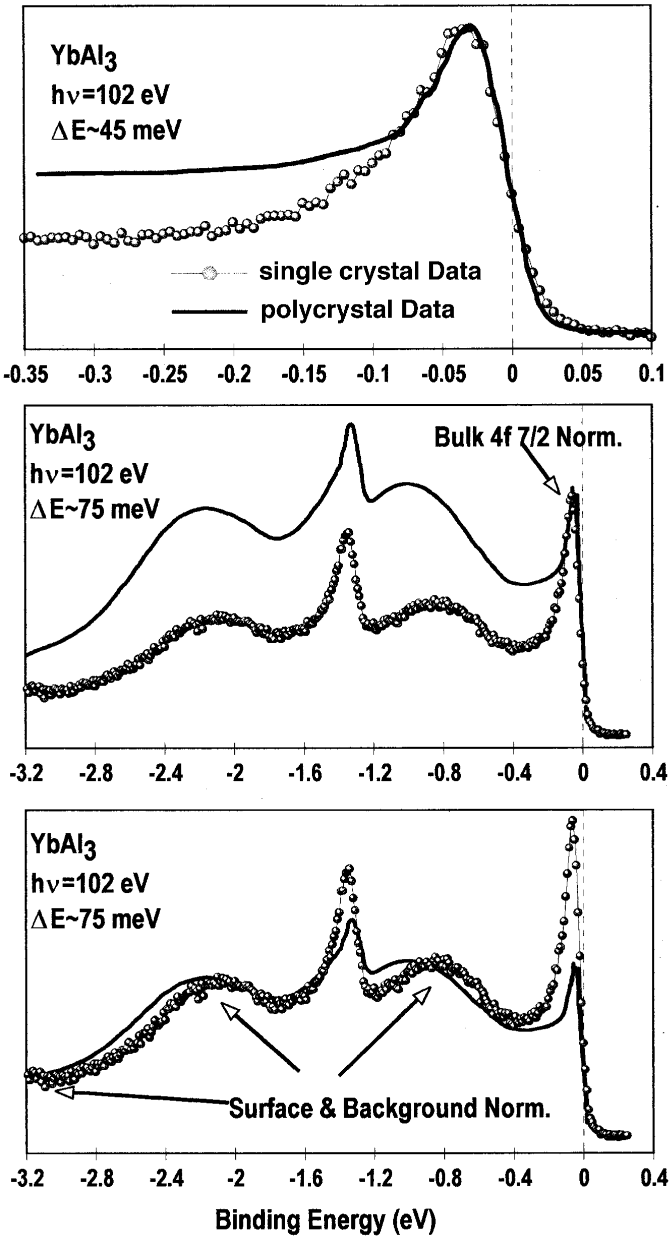

FIG. 12. UPS data for YbAl_3 at $h\nu = 102$ eV with (a) $\Delta E_{\mathrm{ex}} \sim 45$ meV and (b) and (c) $\Delta E_{\mathrm{ex}} \sim 75$ meV. The solid lines are scraped polycrystalline data at $T = 10$ K from Ref. 17 and the shaded circles are our data on cleaved single-crystal samples at $T = 20$ K. (a) 45-meV data showing the Yb bulk $4f_{7/2}$ component in the vicinity of the Fermi level. The data reproduce very well in the leading edge of the Fermi level and through the peak region, indicating that the data are measuring the same spectral feature. The data of Ref. 17 show a smaller peak to valley ratio probably due to the polycrystalline nature of the sample or scraping of the surface, which gives rise to multiple surface configurations and a reduced photoelectron MFP. (b) 75-meV data showing the entire divalent region. The data are normalized to bulk $4f7/2$ peak height. The improved peak to valley ratio in our data leads to a less ambiguous line-shape analysis and a greater percentage of the emission arising from the bulk component for comparison to the trivalent signal in n_f calculations. (c) 75-meV data again showing the entire divalent region; now the data are normalized to surface $4f$ peak height (which also normalizes the backgrounds).

the full divalent $4f$ data forces the bulk $4f_{7/2}$ level near E_F to properly accommodate the surface $4f_{7/2}$ component at slightly deeper binding energy ($E_B \sim 0.8$ eV). Combined with the superior peak to valley ratio of single crystal data, a fit to the full divalent $4f$ emission represents a well-constrained system with a much higher confidence level in the fitted values of the line-shape analysis than limited range fits to data with low peak to valley ratios. Therefore, while both data sets in the top frame of Fig. 12 have slightly better energy resolution than the full divalent $4f$ line-shape analysis presented in Fig. 2 ($\Delta E_{\mathrm{ex}} = 50$ meV), we take the analysis of Fig. 2 to represent the definitive quantitative analysis for the YbAl_3 $4f$ line shape.

The discussion for Fig. 3 dealt with the effects of the Fermi function on a sharply peaked DOS (bulk Yb $4f_{7/2}$ level) in near proximity to the Fermi level using simulated line-shape parameters obtained from fits to Yb metal and YbAl_3. We now consider directly the similarities between this purely divalent material (Yb metal) and the strongly correlated compound YbAl_3. In Fig. 13 we show angle resolved (±1°) UPS data with $\Delta E_{\mathrm{ex}} \sim 75$ meV for Yb metal (black line) and YbAl_3 (shaded circles). In the top frame is the full divalent $4f$ PES signal composed of two spin-orbit-split doublets representing the surface and bulk contributions. The Yb metal spectrum has been offset by ~ 1.2 eV towards the Fermi level so as to overlap the YbAl_3 spectrum for comparative reasons. The middle frame shows an enlargement of the region in the vicinity of E_F that includes the bulk $4f_{7/2}$ component for both materials. There are only two significant differences in the PES spectra for these two materials. First, the YbAl_3 shows a larger portion of the $4f$ emission arising from the surface component than the Yb metal data. This is because the YbAl_3 is mixed valent and the bulk $4f$ emission is split between the divalent and trivalent configurations, whereas the surface emission is purely divalent and arises from all of the surface related Yb atoms in YbAl_3. this difference is therefore inconsequential and is not considered beyond this point. The second notable difference in the PES spectra of the divalent $4f$ levels for these two materials is in the width of the bulk $4f_{7/2}$ component. With the explanation for the bulk to surface ratio above, this difference in the linewidth is all that separates the measured PES $4f$ signature of Yb metal from a strongly correlated material such as YbAl_3. Since the data are taken with the same experimental energy resolution and both samples were at low temperature ($T \sim 20$ K), making the phonon broadening insignificant, the difference between the two line shapes must be due to either a difference in the natural linewidth or the fact that the YbAl_3 $4f_{7/2}$ level is cut by the Fermi function. The middle frame of Fig. 13 shows the differences in the bulk $4f_{7/2}$ levels in detail. In the lower frame the analysis is as follows. We take the Yb film data (solid line in the top two frames) and now show the individual data points in the lower frame as shaded circles. Next we fit the Yb metal data (shaded circles) by the methodologies previously described in the paper using a DS line shape for the natural linewidth. Again, it is observed that the fit (solid line) is of high quality and is well representative of the actual data. Then, we take the natural linewidth for the fitted peak, cut this line shape with a Fermi function centered 21 meV above the DS line-shape peak, and then convolute this line shape with a 75-meV Gaussian function representing the experimental resolution. This Fermi-function-truncated Yb metal fit is displayed as the dot-dashed line in the lower frame. We used a Fermi function 21 meV above the peak of the DS line shape because that was the value determined from the fit to the

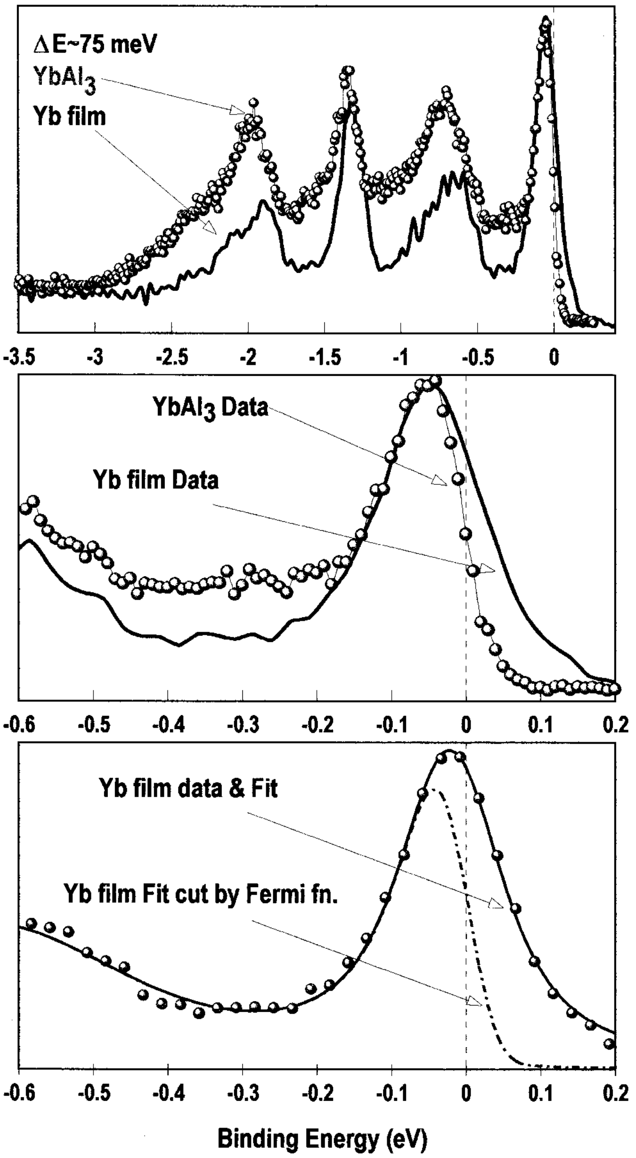

FIG. 13. YbAl_3 and Yb metal UPS data for the divalent Yb $4f$ region with 1° angular acceptance for the electron analyzer and $\Delta E_{\mathrm{ex}} \sim 75$ meV. The Yb metal spectrum has been shifted ~ 1.2 eV toward the Fermi level to overlay the YbAl_3 spectrum. (a) The solid line is Yb metal and the shaded circles are YbAl_3. The similarity in the $4f_{7/2}$ and $4f_{5/2}$ levels of the bulk and surface components is striking. With some of the YbAl_3 bulk $4f$ intensity diverted to the trivalent configuration, the surface to bulk intensity ratio is larger in YbAl_3 than Yb metal, but when this is accounted for, the spectra would be remarkably similar. (b) Detail of the bulk $4f_{7/2}$ and Fermi level region from (a). The major difference is in the emission centered about the Fermi level as the Yb metal data has been shifted and is not effected by the Fermi function like the YbAl_3 data. (c) Yb metal data (circles) and fit to the data (solid line) as in Fig. 1. If the Yb metal data are cut by a Fermi function 21 meV above the $4f_{7/2}$ peak as is YbAl_3, the resulting line shape is the dot-dashed line and compares well with the YbAl_3 $4f_{7/2}$ level in (b).

YbAl$_3$ data in Fig. 2. In the lower frame of Fig. 13, the fit to the Yb metal (solid line) and the Fermi-function-truncated fit (dot-dashed line) are everywhere equal until $\sim$75 meV below the Fermi level; then the effect of the Fermi function becomes more pronounced with increasing energy until approximately one resolution width (75 meV) above the Fermi level where the intensity becomes vanishingly small. The 20-K Fermi function used in this analysis is essentially a step function about the Fermi level on the energy scale of Fig. 13 (the 10% and 90% intensity values are ± 4 meV about the Fermi energy) and therefore the effects of the Fermi function are observed predominantly within $\pm 1 \Delta E_{\mathrm{ex}}$ of E_F. Comparing the fitted and truncated-fitted Yb metal line shapes of the lower frame to the two data sets of the middle frame one is drawn to the inescapable conclusion that, save for the role of the Fermi function, *the PES spectra of the Yb* $4f$ *levels in YbAl*$_3$ *are insignificantly different from the corelike* $4f$ *levels in Yb metal.*

In the Introduction and opening segments of Sec. III, we detailed the normalization procedures used throughout the paper. The method of mesh current normalization (recording an average mesh current either at the start or end of an EDC or both) at a synchrotron facility has several drawbacks, mostly related to orbit changes in the stored particle beam or changes in optical alignment including the photon monochromator, sample position, or energy analyzer, on the time scale of the data acquisition period for one EDC. These pitfalls can be somewhat alleviated by measuring the photon flux at each point in the EDC. The problem with this method is that the mesh current for high-resolution UPS data is generally of a picoampere magnitude (through a 90% transmitting mesh) and the noise associated with this low-current measurement is folded into the noise of the EDC pulse counting statistics resulting in poor signal-to-noise ratios in many circumstances. An additional problem arises when doing mesh normalization for temperature-dependent data. When changing temperatures, expansion or contraction in the cryostat requires realignment of the sample in the photon beam. This realignment could introduce additional errors in the absolute intensity of the measured photoemission signal. While the core-level normalization used throughout most of this paper is generally of greater utility and more easily implemented, we now present point by point photon flux normalized EDC's as this method of normalization gives absolute intensity values if the signal-to-noise ratio and positional instabilities can be mastered.

We present in Fig. 14 temperature-dependent PES data using point-by-point photon flux normalization for Yb metal in the top frame and YbAl$_3$ in the bottom frame. The high-temperature data are the solid line with the low-temperature data as the shaded circles. In both data sets, it is notable that the high-temperature data show a measurable increase in intensity at binding energies beyond the divalent $4f$ emission attributable to secondary electron scattering. If the above normalization does indeed provide an absolute intensity measurement, then the most direct interpretation of these PES results is that the scattering length and thus the mean free path decreases as the temperature increases for these materials. This would be expected from the resistivity of these materials as a function of temperature; however, it has important ramifications for various other methods of normalization particularly if one chooses an arbitrary point in the secondary emission or a valley between surface and bulk components in the divalent emission on which to normalize.[17,18] The results on the point by point flux normalized EDC's are at this time strictly preliminary. However, the increased secondary emission along with the filling in of the valleys between the surface and bulk components both give tangible support to an intuitive notion that the probe depth of photoelectron spectroscopy is not a constant of the measurement temperature and, for the most surface sensitive UPS photon energies, may indeed present a measurable difference in the probe depth with temperature.

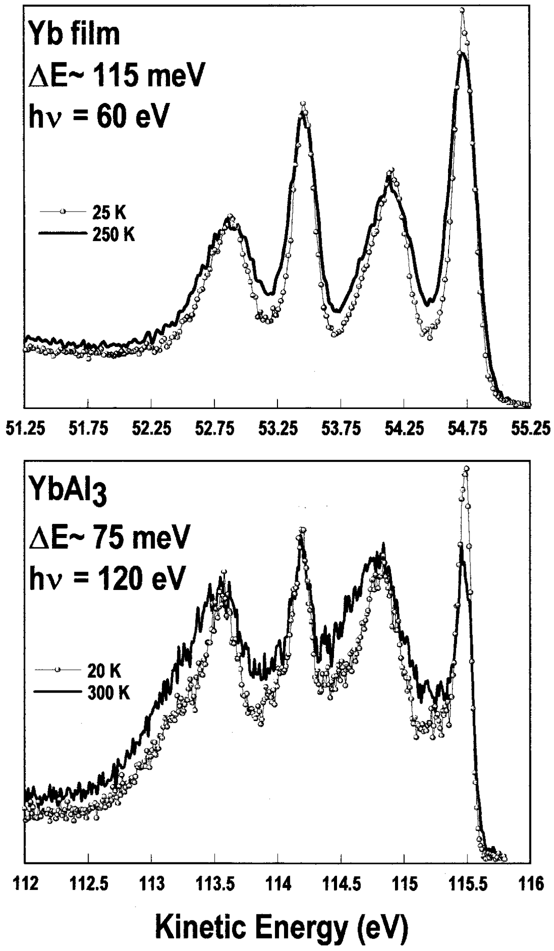

FIG. 14. YbAl$_3$ (bottom) and Yb metal (top) UPS data for the divalent Yb $4f$ region using photon flux normalization to indicate the intensity variation with temperature in these two materials. The total number of counts per energy step was divided by the photon flux (mesh current) taken at each data point. In both cases the higher-temperature spectrum shows a slightly enhanced secondary emission, possibly due to the increased scattering and associated reduction in the mean free path.

IV. CONCLUSION

We have shown that the PES results for the *divalent portion* of strongly correlated Yb-based materials *can* be analyzed within a conventional core-level framework. Deviations from this analysis might well be treated in a perturbative fashion. The question of whether the divalent portion of the $4f$ levels *should* be treated in this manner is another matter, given the clear mixed-valent nature of these Yb compounds. Several points are clear from the PES results and analysis. (i) The width Γ_{DS} of the bulk $4f_{7/2}$ level, which is the peak nearest the Fermi level, is generally $\sim$75 meV for the materials included in this paper (Yb metal, $\mathrm{YbCu_2Si_2}$, $\mathrm{YbAl_3}$, and $\mathrm{YbAgCu_4}$). (ii) The separation of the surface and bulk components in the Yb $4f$ levels ($\Delta E_B \sim 600$ meV) makes characterization of the bulk excited-state f levels unambiguous. (iii) The readily observed multiple surface core-level shifts found in the single-crystal samples [Figs. 6(c) and 8(c)] indicate that surface vs bulk separation is clear-cut in all cases and the Yb $4f$ levels converge to bulk characteristics beyond the first unit cell at the surface. (iv) The consistency between spectral features in the XPS and UPS spectra clearly define the PES data as measuring the bulk excited state properties of these Yb compounds. Also, both the n_f values and the detailed divalent line-shape analysis are in excellent agreement with each other over these two PES regimes. (v) The agreement between the quantitative analysis for the XPS and UPS regimes reinforces the validity of the sudden approximation for these PES results, which is requisite for the Frank-Condon phonon-broadening analysis.

When the body of evidence including the n_f values ($\sim$0.6), the small temperature dependence, the conventional linewidths ($4f_{7/2} \sim 75$ meV), the similarity between $\mathrm{YbAl_3}$ and Yb metal (Fig. 13), and the agreement with the core-level, Fermi-function, phonon-broadening simulation (Figs. 3, 4, 10, and 11) are considered together, conventional mixed-valent models for the PES-determined spectroscopic characteristics seem applicable, raising for consideration the possibility that many of the unique properties of these strongly correlated materials might result from a fortuitous degeneracy between the corelike divalent portion of the $4f$ levels and the Fermi level. Finally, Yb heavy fermions exhibit PES results that seem more consistent with a conventional mixed-valent (with the divalent $4f$ modeled as corelike) interpretation rather than a complex spin fluctuation model[4–6] invoking a narrow, strongly temperature-dependent resonance feature in near proximity to the Fermi level.

ACKNOWLEDGMENTS

This work was supported by the U.S. Department of Energy. The Synchrotron Radiation Center is operated by the University of Wisconsin for the National Science Foundation under Award No. DMR-95-31009 and the National Synchrotron Light Source is funded by the U.S. Department of Energy. We thank John Weaver for providing the facilities for the XPS measurements.

APPENDIX A: HYBRIDIZATION AND HOLE OCCUPANCY

The divalent portion of the Yb $4f$ signal has been described throughout the text as corelike with the suggestion that hybridization with conduction electrons might be treated perturbatively. The analysis of the divalent Yb $4f$ photoemission data within a core-level framework proved quantitatively accurate; however, the implications of hybridization with the conduction states were not addressed in the text as the extent of hybridization between the Yb $4f$ levels and the conduction states was not ascertainable from the PES data. Although the effects of hybridization are not clearly discernible in our Yb PES results, degenerate perturbation theory mandates such hybridization, which will result in a lower-energy ground state. Both the intra-f-level overlap and the hybridization for Yb compounds might be expected to be smaller than for Ce or U compounds. Indeed, the effects of band formation between f levels in the PES data have now been demonstrated in both Ce-based and U-based strongly correlated materials.[19,20,38,45] A manifestation in the PES data of intra-f-level overlap is energy dispersion and periodicity with the crystal lattice. We have, as yet, observed neither the periodicity of the lattice nor dispersion in the $4f$ levels of Yb heavy fermions. This is not surprising since the spatial localization of the Yb $4f$ levels exceeds that of the Ce $4f$ levels or the U $5f$ levels.

Consider the atomic structure calculations of Herman and Skillman[39] as well as those of Freeman.[40] In the rare-earth elements, the radial wave function for the conduction electrons ($5d$ and $6s$) are much larger than those of the $4f$ levels. In fact, comparing the conduction radial wave functions with the Wigner-Seitz radius for metallic rare-earth solids indicates large overlap in the wave functions for adjacent sites. In contrast, the overlap between neighboring sites for the $4f$ wave functions is extremely small.[41] This leads to two suppositions: first, the band formation in the f levels is weak (as indicated in Ce $4f$ and U $5f$ dispersions of order 50 meV) and, second, the mismatch in radial wave functions leads to low hybridization between the f levels and the conduction states. The peak in the radial wave function for the $4f$ level of Yb is 50% smaller than that of Ce (0.24 Å vs 0.36 Å). This might lead one to conclude that the hybridization in Yb correlated electron materials is generally smaller than for Ce-based materials. Also, the dispersion of the $4f$ levels one might expect to observe would be commensurately less than the 50 meV observed for Ce heavy fermions (very likely below the detectable level of a PES apparatus). Nevertheless, hybridization of the $4f$ levels in Yb would lift the ground-state degeneracy of the $4f$ level (as would consideration of relativistic effects in the Yb $4f$ levels, which are of order 10% of the $4f$ energy within the relativistic mass-velocity correction[39]). So, while we are currently not able to directly observe the effects of hybridization in the PES of these Yb materials, the consideration of hybridization in the interpretation of these Yb materials should not be ignored.

The PES measurements of n_f values ($\sim 0.6 - - 0.65$) for the Yb heavy fermions presented in the text place these materials in the mixed-valent regime of strongly correlated materials (and well outside of the SIAM regime). We indicated the role of the Fermi function and phonon broadening in reducing the divalent $4f_{7/2}$ intensity as a function of temperature. It should not be surprising that in addition to the Fermi-function–phonon-broadening role, the balance between the divalent and trivalent $4f$ ground states could also be temperature dependent. Specifically, with the divalent and trivalent ground states almost energetically degenerate (in a traditional mixed-valent model), the lattice changes as a function of temperature could easily lead to a shift in the balance between the weightings of the divalent and trivalent configurations with temperature. These lattice changes are non-negligible for the Yb heavy fermions presented in the text. For $YbCu_2Si_2$ the $\Delta l/l \sim 0.1\%$ between 80 and 300 K gives rise to a volume change of order 0.3% with a thermal expansion coefficient α ranging from -3×10^{-6}/K at 20 K to 11×10^{-6}/K at 200 K.[42] For $YbAl_3$ the $\Delta l/l \sim 0.065\%$ (Ref. 43) between 173 and 300 K that is comparable to that of $YbCu_2Si_2$, and for $YbAgCu_4$, α ranges from -8×10^{-6}/K at 20 K to 13×10^{-6}/K at 300 K.[44] With lattice changes of this magnitude, one would actually expect variations in the divalent or trivalent intensities as a function of temperature. These types of changes could easily account for divalent $4f$ intensity variations that might be outside of the region (bulk $4f_{7/2}$ level) covered by the Fermi-function–phonon-broadening method detailed in the text.

APPENDIX B: SINGLE CRYSTALS, SIAM, AND THE CORRELATED ELECTRON PROBLEM

The heavy-fermion PES community had, by necessity, made extensive use of polycrystalline samples in the 1980s. In the 1990s, single-crystal samples of sufficient size for PES measurements became available for several Ce, Yb, and U-based heavy fermions. Presently, both cleaved single crystals and scraped polycrystals are used in heavy-fermion PES experiments by different groups. It has been observed that the cleaved single-crystal PES results are sometimes different from the scraped polycrystalline counterparts.[15,17,18] The nature of this discrepancy will be discussed for two particular Yb heavy-fermion systems and the merits of cleaved single-crystal PES for Yb as well as Ce and U heavy-fermion systems will be outlined and referenced.

The two Yb-based heavy-fermion systems under consideration are $YbAl_3$ and $YbAgCu_4$. For both materials, there are published polycrystalline results that show a temperature dependence and are interpreted within the SIAM. There are at least two similarities between these polycrystalline $YbAl_3$ (Ref. 17) and $YbAgCu_4$ (Ref. 18) papers: both papers report a temperature dependence in excess of what is reported here and both papers make similar choices for the non-bulk-$4f_{7/2}$ intensity of the PES signal. The differences between the PES results fall into two categories: actual, measured experimental data and quantitative results arising from data analysis. There do indeed appear to be differences in the actual, measured experimental data previously reported and the current work. These differences will be considered subsequent to the analysis discussion.

Both the $YbAl_3$ and $YbAgCu_4$ polycrystalline PES papers show temperature-dependent, high-resolution, surface-sensitive photoemission of the bulk $4f_{7/2}$ components in the immediate vicinity of the Fermi level ($YbAl_3$, Ref. 17, Fig. 2 and $YbAgCu_4$, Ref. 18, Fig. 2). In both cases, the authors have separated the portion of the PES signal arising from the bulk Yb $4f_{7/2}$ component (the so-called Kondo resonance) and the remainder of the PES signal (secondary emission, surface $4f$, and non-f emission). Also, in both papers, an n_f value or spectral intensity is calculated using this temperature dependence of the ''Kondo resonance'' ($YbAl_3$, Ref. 17, Fig. 4 and $YbAgCu_4$, Ref. 18, Fig. 3). While the analysis in these papers is self-consistent, there could arise a problem if the analysis used to determine the temperature dependence and thus the n_f value were in need of revision. Therefore, irrespective of the raw data differences between past and present work, if the analysis of these previous two data sets were to yield significantly different bulk Yb $4f_{7/2}$ components in the PES signal, one would no longer have conformity to the noncrossing approximation results for the temperature dependence or hole occupancy in conformity with the SIAM (since both papers claim good agreement with SIAM using the published line-shape analysis).

While there may be no absolute right or wrong line-shape analysis for the $4f$ levels in these Yb-based heavy fermions, there are ranges of values that are acceptable and other values outside of this range where one might question the physical meaning of the parameters or line shapes. With this in mind, one might consider that the above-cited Yb heavy-fermion papers, irrespective of any actual temperature dependence measured, would indeed not conform to the SIAM predictions if the determination of the bulk $4f_{7/2}$ level included consideration of the peak-to-valley and bulk-to-surface ratios inherent in the Yb $4f$ data presented in the present work. Specifically, the Yb $4f$ results reported in the present paper yield peak-to-valley and bulk-to-surface ratios substantially larger than those reported previously.[17,18] These larger ratios allow for smaller error bars in the analysis as well as increased confidence levels in the fitted values. Moreover, these larger ratios serve to constrain the fitting parameters to a much smaller subset of parameter space than the data presented in Refs. 17 and 18 and, in particular, the contribution to the total spectral intensity within 100 meV of E_F from the bulk $4f_{7/2}$ level is substantially greater than that reported in these polycrystal papers.[17,18]

In the top frame of Fig. 15 are single-crystal and polycrystal PES results for $YbAl_3$. This same polycrystal data[17] was shown in Fig. 12, while the single-crystal data are from Refs. 15 and 16. The dot-dashed line is the preferred nonbulk $4f_{7/2}$ background chosen from the analysis in Ref. 17. While this background might conceivably be possible (for the near Fermi-level region as used in Ref. 17) if one considers only the polycrystalline data set, comparison to the single-crystal data for $YbAl_3$ would allow one to rule out this ''background B'' as an option for the nonbulk $4f_{7/2}$ background. This background B, if applied to the single-crystal data, would truncate nearly two-thirds of the actual $4f_{7/2}$ level (indicated in the top frame by the dashed line). Moreover, it is plainly obvious that if one were to truncate the majority of the Yb $4f_{7/2}$ level reported in this paper in the same fashion, the temperature dependences in the present paper (Fig. 4 for $YbAl_3$, Fig. 10 for $YbCu_2Si_2$, and Fig. 11 for $YbAgCu_4$) would look commensurately larger and much more like the temperature dependences reported in Refs. 17 and 18. The analysis presented throughout this paper has shown that this type of background determination would not be accurate for the single-crystal data presented.

The above comparison raises the question as to which method of analysis is more appropriate. We contend that the methodologies that were used throughout this manuscript are sound and lead to physically reasonable analytical results. Specifically, the analysis used throughout the present work explicitly and quantitatively accounted for the ligand emission in the PES signal (Lu and La isoelectronic counterparts) as well as the surface contributions to the PES. Additionally, the secondary backgrounds were determined by standard

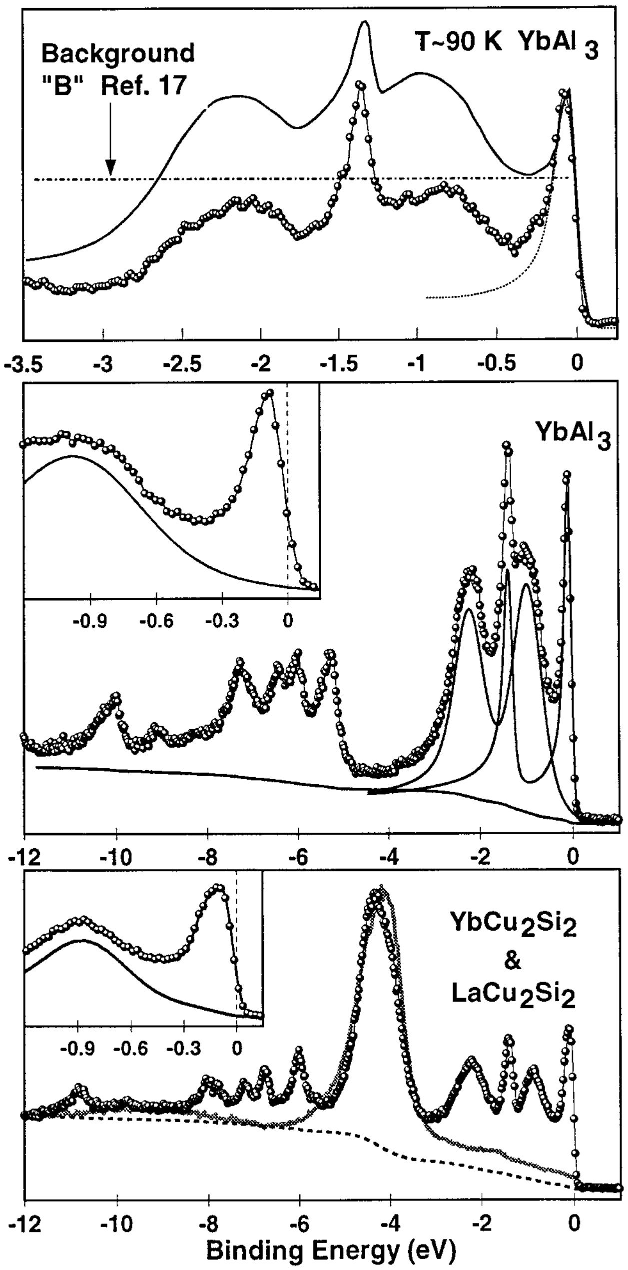

FIG. 15. $YbAl_3$ and $YbCu_2Si_2$ UPS data. (a) Comparison of single-crystal vs polycrystal $YbAl_3$ PES data of Ref. 17 (line, $T\sim100$ K, $h\nu=102$ eV) and Ref. 16, Fig. 8 (circles, $T\sim80$ K, $h\nu=120$ eV) originally presented in Fig. 1 of Ref. 15. The dot-dashed horizontal line is the nonbulk $4f$ background B of Ref. 17 and the dotted line is the single crystal $4f_{7/2}$ bulk fitted component. The superior peak to valley ratio for the single-crystal data greatly improves the confidence factor in the line-shape analysis. (b) $YbAl_3$ PES data at $T\sim80$ K and $h\nu=120$ eV, showing the full valence-band background and the surface and bulk contributions to the Yb $4f$ signal. (c) $YbCu_2Si_2$ UPS data (circles), $LaCu_2Si_2$ data (gray line), and the full valence-band integral background (dashed line) showing the breakdown into various $4f$ and non-$4f$ contributions to the total PES signal.

methods and applied over the entire valence-band region. The full valence-band scan presented in the middle frame of Fig. 15 is the same as that presented in Fig. 7. In addition, the line-shape analysis and the data for the Fermi level region are presented in the inset to indicate the nonbulk $4f_{7/2}$ background for single-crystal $YbAl_3$. Now it is clearly that the intensity just below the Fermi level is completely dominated by the bulk $4f_{7/2}$ level. Moreover, one may determine directly the hole occupancy for the material from the full valence-band spectra by direct analysis rather than combining two different spectroscopies (XAS and PES) measured at different times as was done for $YbAl_3$ in Ref. 17. Also, the full valence-band scans allow one to directly monitor contamination levels as the sample temperature changes or the sample surface ages. It is clear from the temperature-dependent data of Fig. 4 that there was no contamination problem at any temperature for the single-crystal $YbAl_3$ results. The wide valence-band scans and Al $2p$ core-level normalization incorporated (via second order) into these valence-band scan presents a nearly complete picture for the temperature dependence. The only additional information one might realistically want would be surface structural information. Namely, was there an ordered surface structure at both temperatures and was it the same structure? To collect these data (low-energy electron diffraction or reflection high-energy electron diffraction) in addition to the PES data within the sample lifetime is beyond the present scope of our experimental setup. Perhaps these data could be collected independently, and if found to be highly reproducible, extrapolated onto the PES findings. Of course, this type of information is not possible with polycrystals since there is no long-range order at the surface to track.

In the lower frame of Fig. 15 we show that the analysis used for $YbAl_3$ is, in fact, general and applicable to all of the Yb heavy fermions we have studied. The lower frame shows the analysis for $YbCu_2Si_2$ with the ligand emission determined from $LaCu_2Si_2$ and the secondary emission again analyzed over the entire valence-band region. Although there is more ligand intensity in this material than the previous material, the inset shows the intensity at the Fermi level is once again dominated by the bulk $4f_{7/2}$ level. If one examines the nonbulk $4f_{7/2}$ background for the polycrystal determined in the top frame of Fig. 15 and compares it to the nonbulk $4f_{7/2}$ background determined in the lower two frames of the same figure for the single-crystal data, one can see that a good deal of the differences reported in the literature on the same material arises from different analysis. We contend that our analysis is more reliable because: (i) the peak-to-valley ratio for the bulk $4f_{7/2}$ level is larger in our data and allows us to fit the data more reliably, (ii) the bulk-to-surface ratio is larger in our data and allows for a higher confidence level in the parameters determined from the least-squares minimization, (iii) we have accurately removed the ligand emission from the PES spectrum by measuring La and Lu counterparts to the Yb heavy fermions presented in this paper, (iv) the secondary electron emission has been properly accounted for by examining the full valence band including the entire divalent and trivalent $4f$ signals, and (v) contamination levels are directly monitored in our full valence-band scans at each temperature.

The results for $YbAgCu_4$ presented in Ref. 18 and this paper are not as different as the single-crystal vs polycrystal $YbAl_3$ results. This is probably because both groups used polycrystals for $YbAgCu_4$ and both groups fractured the sample to prepare the surface rather than scraping the surface. Our $YbAgCu_4$ was a large grain growth with visually prominent single-crystal domains. The microstructure of the $YbAgCu_4$ used in Ref. 18 was not detailed in the text of that paper so we do not know if their samples differ significantly in microstructure from ours, although the growth method was clearly different. In fact, the authors of Ref. 18 also scraped the sample surface and found the following: ''The intensity ratio of bulk to surface features however was always less favorable than in the case of the broken sample.'' This has been our finding also whenever scraping is used for sample surface preparation. There is again in these two data sets a difference in analysis that significantly effects the interpretation of the temperature dependence for $YbAgCu_4$. Our analysis parallels that detailed above for the case of $YbAl_3$. Again we have full valence-band scans and a Lu isoelectronic for ligand removal. Once again our peak-to-valley ratio is better for the peak near the Fermi level [Fig. 11(b) vs Fig. 2 for Ref. 18], but this time the discrepancy is not as large. In this case, although the energy resolution is 2.5 times better in Ref. 18 than our 60-meV resolution in Fig. 11(b), our peak-to-valley ratio is still larger probably due to the larger Yb $4f$ cross section at 60 eV vs the 40.8 eV energy used in Ref. 18. One other possibility for the difference could be sample preparation, although this is pure speculation. Our samples were grown enclosed in sealed Ta to maintain the Yb stoichiometry, whereas Ref. 18 reports argon arc furnace growth that can lead to Yb depletion due to its large vapor pressure at elevated temperatures.

As in the case for $YbAl_3$, we have full valence-band scans to monitor sample surface integrity as a function of temperature and inclusion of the trivalent Yb $4f$ signal again makes determination of the n_f value possible from the same spectrum. We find an n_f value of 0.65 for $YbAgCu_4$, well outside the Kondo regime. One must also consider in the analysis that which might initially seem to be part of the raw data discrepancy, namely, normalization. How does one normalize the data between different temperatures? As discussed in the text with respect to Fig. 14, the answer to this seemingly obvious question is not even clear.

It is our opinion that determining the temperature dependence of the bulk $4f$ levels from surface sensitive PES data is the most difficult of the $4f$ measurements. It is somewhat simpler to obtain values of the $4f$ binding energy, linewidth, and hole occupancy (n_f) because these values can all be obtained from a single spectrum rather than normalizing multiple spectra and then trying to account for possible changes in surface structure or surface contaminants. With this in mind, we state that the temperature dependences observed for the Yb heavy fermions reported in this paper are in the 0–10 % range. That is, in addition to some small differences between the various Yb materials, there are also small variations within a given material. Specifically, some cleaves on YbAl, and $YbCu_2Si_2$ show almost no temperature dependence at all, while other cleaves can show up to 10% variation with temperature. It is not clear whether the range of values for the temperature dependence is due to inherent variations in intensity normalization or actual sample variations that include surface preparation techniques. Having conducted well over a dozen temperature studies on each of these two Yb heavy fermions, the possibility of significant revision on the 0–10 % temperature variation with temperature seems unlikely.

Having studied both single crystals and polycrystals using PES, we have found the single-crystal results to be more reliable. This reliability of single crystals arises from (i) a small percentage of the signal attributed to surface emission, (ii) a more stable surface against reaction than polycrystals, (iii) no inclusions of second phases in the flux grown samples, and (iv) no grain boundaries for internal contamination or migration of elements. Also, in the case of temperature dependence, there may be many possible explanations for variations in intensity with temperature, but there are very few explanations for little or no temperature dependence. Therefore, if there are two sets of data, one showing little temperature dependence on single crystals and another showing larger temperature dependence on the polycrystals, we would contend that the single-crystal results in this case are more likely to reflect the intrinsic properties of the material under investigation.

While the main body of this paper was devoted to PES results and analysis without detailed discussion on applicable models, we now state that the Yb results reported in this work are indeed incompatible with the many predictions of the SIAM. Moreover, the $YbAgCu_4$ results in Ref. 18 report a linewidth and binding energy for the Kondo resonance completely inconsistent with the SIAM, but in full agreement with the original report of the $4f$ linewidth and binding energy for $YbAgCu_4$.[37] It might also be the case that if a more conventional background were chosen in Ref. 17, the results of that paper would also yield values for the PES inconsistent with the SIAM.

There are even more compelling reasons to abandon the SIAM as an explanation for heavy-fermion characteristics and these reasons have their roots in the single-crystal PES data for Ce and U-based heavy fermions. It has been shown that the bulk Ce $4f$ levels in $CeBe_{13}$ (Ref. 20) and $CePt_{2x}$ (Ref. 19) are periodic with the lattice. That is, the bulk $4f$ spectral intensity modulates with the reciprocal lattice vector, giving clear indication that the $4f$ levels are bands and not fully localized impurities. This work was performed at the Ce resonance energy of 120 eV. Further research on USb_2 (Ref. 38) and UPt_3 (Ref. 45) was conducted at lower photon energies yielding even higher-energy resolution (35 meV) but also much better **k**-space resolution ($\frac{1}{10}$ of the Brillion zone in the Γ-X direction). With this improved energy and **k**-space resolution one now plainly observes dispersion in the f level as well as the intensity modulation reported for Ce at higher photon energies.

In summary, the SIAM has been shown to be fundamentally at odds with the experimental results for Ce and U heavy fermions. The dispersion of the f levels in Ce and U heavy fermions mandates the use of single-crystal samples. If one expects the interesting electronic properties of Yb heavy fermions to be related to the Ce and U-based heavy fermions (as thermodynamic and transport considerations would indicate), then clearly one would want to use single-crystal samples for meaningful Yb heavy-fermion PES studies. While the **k**-dependent PES results for Ce and U f levels makes the SIAM fundamentally inappropriate for explaining the physics of these heavy fermions, one need not abandon the Anderson Hamiltonian as a starting point for correlated electron physics. There are several models based on the

Anderson Hamiltonian that hold promise for explaining the experimental results for Ce, U, and Yb-based heavy fermions. A most promising model has recently been put forth by Sheng and Cooper,[46] which is based on two temperature-independent bands. This model explains the balance between magnetism and the heavy-fermion singlet-ground-state, thermodynamic results (susceptibility and specific heat) and the dispersion and conventional temperature dependence observed in the PES results for both Ce and U heavy fermions. One might also look to the periodic Anderson model,[47] which can show (for certain parameter sets) a much slower temperature dependence than SIAM and also might account for the dispersion observed in PES data. There are many possibilities for explaining or understanding the nature of heavy-fermion behavior, but it would appear that the SIAM is no longer a viable contender. As is often the case, the early front runner (SIAM) for understanding the problem is based on early data and often cannot provide the final explanation when more detailed experimental results become available.

---

[*] Present address: Elettra, Basovizza 34012, Trieste, Italy.

[†] Present address: Hewlett-Packard Corp., Eugene, OR 97402.

[‡] Present address: Physical Electronics Corp., Eden Prairie, MN 55344.

[1] F. Gerken, A. S. Flodtröm, J. Barth, L. I. Johansson, and C. Kunz, Phys. Scr. **32**, 43 (1985).

[2] J. W. Allen, S.-J. Oh, O. Gunnarsson, K. Schönhammer, M. B. Maple, M. S. Torikachvili, and I. Lindau, Adv. Phys. **35**, 275 (1986).

[3] F. Patthey, J.-M. Imer, W.-D. Schneider, H. Beck, and Y. Baer, Phys. Rev. B **42**, 8864 (1990).

[4] O. Gunnarsson and K. Schönhammer, Phys. Rev. B **28**, 4315 (1983).

[5] O. Gunnarsson and K. Schönhammer, Phys. Rev. B **31**, 4815 (1985).

[6] N. E. Bickers, D. L. Cox, and J. W. Wilkins, Phys. Rev. B **36**, 2036 (1987).

[7] T.-C. Chiang, J. A. Knapp, M. Aono, and D. E. Eastman, Phys. Rev. B **21**, 3513 (1980).

[8] H. J. Levinson, F. Greuter, and E. W. Plummer, Phys. Rev. B **27**, 727 (1983).

[9] F. J. Himpsel, Adv. Phys. **32**, 1 (1983).

[10] P. W. Anderson, Phys. Rev. Lett. **18**, 1049 (1967); Phys. Rev. **164**, 352 (1968).

[11] S. H. Liu, *Handbook on the Physics and Chemistry of Rare Earths* (North-Holland, Amsterdam, 1993), Vol. 17, Chap. 111, pp. 87–148.

[12] M. R. Norman, Phys. Rev. B **31**, 6261 (1985); M. R. Norman, D. D. Koelling, and A. J. Freeman, *ibid.* **31**, 6251 (1985).

[13] J. J. Joyce, A. J. Arko, J. M. Lawrence, P. C. Canfield, Z. Fisk, R. J. Bartlett, and J. D. Thompson, Phys. Rev. Lett. **68**, 236 (1992).

[14] J. J. Joyce and A. J. Arko, Phys. Rev. Lett. **70**, 1181 (1993).

[15] J. J. Joyce, A. J. Arko, A. B. Andrews, and R. I. R. Blyth, Phys. Rev. Lett. **72**, 1774 (1994).

[16] J. J. Joyce *et al.*, Physica B **186-188**, 31 (1993).

[17] L. H. Tjeng *et al.*, Phys. Rev. Lett. **71**, 1419 (1993); **72**, 1775 (1994).

[18] P. Weibel, M. Grioni, D. Malterre, B. Dardel, Y. Baer, and M. Besnus, Z. Phys. B **91**, 337 (1993).

[19] A. B. Andrews, J. J. Joyce, A. J. Arko, J. D. Thompson, J. Tang, J. M. Lawrence, and J. C. Hemminger, Phys. Rev. B **51**, 3277 (1995).

[20] A. B. Andrews, J. J. Joyce, A. J. Arko, Z. Fisk, and P. S. Riseborough, Phys. Rev. B **53**, 3317 (1996); A. B. Andrews, J. J. Joyce, A. J. Arko, J. D. Thompson, Z. Fisk, J. Tang, J. M. Lawrence, P. S. Riseborough, and P. C. Canfield, Physica B **206& 207**, 83 (1995).

[21] M. Bodenbach, A. Höhr, C. Laubschat, and G. Kaindl, Phys. Rev. B **50**, 14 446 (1994).

[22] For a general discussion on core-level line-shape analysis see, for example, J. J. Joyce, M. del Giudice, and J. H. Weaver, J. Electron. Spectrosc. Relat. Phenom. **49**, 31 (1989); G. K. Wertheim and S. B. Dicenzo, *ibid.* **37**, 57 (1985).

[23] D. A. Shirley, Phys. Rev. B **5**, 4709 (1972).

[24] S. Doniach and M. Sunjic, J. Phys. C **3**, 285 (1970).

[25] D. M. Riffe, G. K. Wertheim, and P. H. Citrin, Phys. Rev. Lett. **63**, 1976 (1989).

[26] P. H. Citrin, G. K. Wertheim, and Y. Baer, Phys. Rev. B **16**, 4256 (1977).

[27] The single-crystal PES results from Ref. 21 seem to be in good agreement with our evaporated thin-film results. We converged on the present spectra by doing evaporation at several different temperatures and then several different ''annealings'' of the film before considering the present line shapes to be representative of the true electronic structure of Yb metal. The single-crystal results show a difference in the SCS, but the linewidths seem quite similar. We observe the same results for YbAl$_3$, where the best polycrystalline samples show the correct linewidth, but generally are dominated by surface and secondary-electron contributions compared to single-crystal results.

[28] D. M. Riffe, G. K. Wertheim, D. N. E. Buchanan, and P. H. Citrin, Phys. Rev. B **45**, 6216 (1992).

[29] R. I. R. Blyth *et al.*, Phys. Rev. B **48**, 9497 (1993).

[30] P. H. Citrin, G. K. Wertheim, and Y. Baer, Phys. Rev. B **27**, 3160 (1983).

[31] J. J. Joyce *et al.*, Physica B **205**, 365 (1995).

[32] G. K. Wertheim and P. H. Citrin, Phys. Rev. B **30**, 4343 (1984).

[33] G. K. Wertheim and P. H. Citrin, Phys. Rev. B **38**, 7820 (1988).

[34] The n_f value of 0.63 is in good agreement with the findings of Ref. 35, but greatly at odds with the value obtained in Ref. 17. Interestingly, Refs. 35 and 17 share the same high-resolution PES data for YbAl$_3$, but end up with different values of n_f.

[35] S.-J. Oh, Phys. Physica B **186-188**, 26 (1993).

[36] En-Jin Cho *et al.*, Phys. Rev. B **47**, 3933 (1993).

[37] J. J. Joyce, Bull. Am. Phys. Soc. **37** (1), 637 (1992); Philos. Mag. Lett. (to be published).

[38] A. J. Arko, J. J. Joyce, A. B. Andrews, D. Mandrus, E. Moshopoulou, Z. Fisk, and P. C. Canfield (unpublished).

[39] F. Herman and S. Skillman, *Atomic Structure Calculations* (Prentice-Hall, Englewood Cliffs, NJ, 1963).

[40] A. J. Freeman, Physica B **102**, 3 (1980).

[41] The radial wave functions for Gd are shown in Ref. 40, Fig. 1, along with the Wigner-Seitz radius for metallic Gd. The agreement between the radial wave functions for Refs. 39 and 40 is excellent. From Ref. 39, the peak in the radial wave function for Ce and U are substantially larger than for Yb.

[42] Y. Uwatoko, G. Oomi, J. D. Thompson, P. C. Canfield, and Z. Fisk, Physica B **186-188**, 593 (1993).

[43] A. Iandelli and A. Palenzona, J. Less Common Metals **29**, 293 (1972).

[44] J. M. Lawrence *et al.* (private communication).

[45] A. J. Arko, J. J. Joyce, A. B. Andrews, J. L. Smith, E. Moshopoulou, Z. Fisk, and P. C. Canfield, Physica B (to be published).

[46] Q. G. Sheng and Bernard R. Cooper, Philos. Mag. Lett. **72**, 123 (1995).

[47] M. Jarrell, Phys. Rev. B **51**, 7429 (1995); M. Jarrell (private communication).